Carcinogens transform into electrophilic metabolites, bind to DNA, and cause cancer via metabolic activation, detoxification, angiogenesis, and metastasis. CYP isozymes are therapeutic targets in DBP-induced mammary cancer. LBVS, molecular docking, MD simulations, and in vitro studies have focused on CYP1A1, 1A2, and 1B1. LBVS identified hits, refined using Lipinski's RO5 and ADMET filters, and docked them using AutoDock4. CHEMBL1, CHEMBL2, and CHEMBL3 showed superior binding affinities to ANF. The stability was confirmed via MD simulations. ADMET filtering yielded nontoxic hits, with ANA8430692 and ANA7923580 exhibiting optimal stability. Molecular dynamics and enzyme inhibition assays validated their potential as CYP inhibitors. Designed analogs ANA6917483, ANA8430692, and ANA6451816 displayed strong binding and interaction patterns, suggesting anticancer potential. This study enhances our understanding of the DBP-induced prevention of mammary cancer.

Dr. Mohammad Kalim Ahmad Khan, a Professor of Bioinformatics in the Department of Bioengineering at Integral University, Lucknow, India, has 16+ years of experience, 85+ publications, and has supervised six PhD scholars. His research focuses on DB[a,l]P-induced carcinogenesis, lifestyle diseases, and computational design of drug candidates.

9 7 8 6 2 0 8 4 1 7 1 5 4

Ahmad Khan, Akhtar, Azeem

Mohammad Kalim Ahmad Khan
Salman Akhtar
Mohd Umar Azeem

Modulating CYP450 Isozymes to Prevent DB[a,l]P-Induced Mammary Cancer

LAP LAMBERT Academic Publishing

Mohammad Kalim Ahmad Khan
Salman Akhtar
Mohd Umar Azeem

Modulating CYP450 Isozymes to Prevent DB[a,l]P-Induced Mammary Cancer

Mohammad Kalim Ahmad Khan
Salman Akhtar
Mohd Umar Azeem

Modulating CYP450 Isozymes to Prevent DB[a,l]P-Induced Mammary Cancer

LAP LAMBERT Academic Publishing

Imprint
Any brand names and product names mentioned in this book are subject to trademark, brand or patent protection and are trademarks or registered trademarks of their respective holders. The use of brand names, product names, common names, trade names, product descriptions etc. even without a particular marking in this work is in no way to be construed to mean that such names may be regarded as unrestricted in respect of trademark and brand protection legislation and could thus be used by anyone.

Cover image: www.ingimage.com

Publisher:
LAP LAMBERT Academic Publishing
is a trademark of
Dodo Books Indian Ocean Ltd. and OmniScriptum S.R.L publishing group

120 High Road, East Finchley, London, N2 9ED, United Kingdom
Str. Armeneasca 28/1, office 1, Chisinau MD-2012, Republic of Moldova, Europe
Managing Directors: Ieva Konstantinova, Victoria Ursu
info@omniscriptum.com

Printed at: see last page
ISBN: 978-620-8-41715-4

TABLE OF CONTENT

LIST OF TABLES

LIST OF FIGURES

LIST OF SYMBOLS AND ABBREVIATIONS

ADMET	Absorption, Distribution, Metabolism, Excretion, Toxicity
ADT	AutoDock Tools
LBVS	Ligand-Based Virtual Screening
CADD	Computer-Aided Drug Design
MD	Molecular Dynamics
MTT	(3-[4, 5-dimethyl thiozol-2yl]-2yl]-2,5-diphenyl tetrazolium bromide)
RCSB PDB	Research Collaboratory for Structural Bioinformatics Protein Data Bank
Ki	Inhibition Constant
ΔG	Free energy of binding
Rg	Radius of Gyration
RO5	Lipinski Rule of Five
CYP450	Cytochrome P450
ANF	Alpha-naphthoflavone
RMSD	Root Mean Square Deviation
RMSF	Root Mean Square Fluctuation
SASA	Solvent Accessible Surface Area
HIA	Human Intestinal Absorption
BBB	Blood Brain Barrier
PPB	Plasma Protein Binding
MDCK	Madin-Darby Canine Kidney
Caco2	Colorectal Adenocarcinoma
MW	Molecular weight
HBD	Hydrogen Bond Donor
HBA	Hydrogen Bond Acceptor
LogP	Lipophilicity
GPF	Grid Parameter File
DPF	Docking Parameter File

GLG	Grid Log File
DLG	Docking Log File
ns	Nanosecond
ps	Picosecond
kcal/mol	kilocalorie per mole
DSV	Discovery Studio Visualizer

ABSTRACT

The general mechanism of cancer encompasses the metabolism of carcinogens to highly electrophilic metabolites capable of binding to DNA and other macromolecules, thereby initiating cellular transformation. As the carcinogenesis mechanism is highly complex, involving diverse cellular mechanisms in cancer promotion and progression, elucidating the various underlying processes presents a significant challenge. Extensive research into the multifaceted nature of cancer initiation and development, along with associated risk factors and modulators, has resulted in the identification of numerous molecular and cellular markers specific to different cancer types. Nearly all exogenous compounds entering cells are metabolized by phase I and phase II enzymes. During the biotransformation of pro-carcinogens and other xenobiotics, the activation of phase I enzymes and suppression of phase II enzymes are necessary for the manifestation of their mutagenic, toxic, or carcinogenic effects. Metabolic activation, detoxification, cellular proliferation, programmed cell death, angiogenesis, and metastasis have been implicated in target-specific pathways leading to the elucidation of oncogenic mechanisms. The interaction of parent xenobiotics with a particular target can positively, negatively, or neutrally influence their respective cellular pathways. Cytochrome P450 (CYP) isozymes are promising therapeutic targets against dibenzo[a,l]pyrene-induced mammary cancer.. This study aimed to identify potential lead molecules against mammary cancer-targeting CYP1A1, 1A2, and 1B1 using ligand-based virtual screening (LBVS), molecular interactions, molecular dynamics (MD) simulation, and in vitro studies. The LBVS methodology predicted 30,500 hits, which were subsequently reduced to 400 through filtration using Lipinski's Rule of Five (RO5) and ADMET parameters. These 400 compounds were subsequently subjected to molecular docking with the selected CYP isozymes. The ligands CHEMBL224064

(CHEMBL1), CHEMBL2420083 (CHEMBL2), and CHEMBL61745 (CHEMBL3) exhibited stronger binding affinities in CYP1A1 (-10.52 kcal/mol), 1A2 (-10.82 kcal/mol), and 1B1 (-10.78 kcal/mol), respectively, in comparison to the known inhibitor alpha-naphthoflavone (ANF) (-9.13 kcal/mol, -9.66 kcal/mole, and -9.67 kcal/mol in CYP1A1, 1A2, and 1B1, respectively). These compounds demonstrated stability with their respective targets during MD studies of 50 ns duration.

Furthermore, (3-(4, 5-dimethyl thiazolyl-2)-2, 5-diphenyltetrazolium bromide) (MTT) and enzyme inhibition assays were performed to elucidate and validate the inhibitory potential of the identified ligands against mammary carcinomas. Moreover, combinatorial design, computational ADMET, molecular docking, and MD studies were conducted to identify potent inhibitors for CYP1A1, 1A2, and 1B1. Initially, ANF was employed as a template for screening and docking into the active site of CYP450 isozymes for binding mode analysis. Analogs exhibiting optimal interactions with the target protein were subjected to molecular dynamics (MD) simulations for 30 ns. Comparable hydrogen bonding interactions and occupancy were observed during the 30 ns simulations. These findings provide an appropriate starting point for further screening of chemical drug-likeness combinatorial design of substrate analogs. Nontoxic molecules (as determined by carcinogenicity and mutagenicity in rat models) were selected from 400 screened hits. The application of Lipinski's Rule of Five yielded 88 molecules that adhered to three out of four rules. ADME filters were also applied to nontoxic filtered molecules using criteria such as solubility, absorption, polar surface area, and blood-brain barrier permeability. This process resulted in 56 hits in the combinatorial library. Molecular docking studies were conducted using AutoDock4.0 tools. The optimal docked conformation was selected based on criteria including

hydrogen bonding interactions with active-site residues, binding energy, and best fit into the active site of target proteins. Subsequently, the top ten hits against each isozyme were compared with DBPD and ANF. These hits demonstrated stronger binding with their respective isozymes compared to carcinogens and known inhibitors. Furthermore, MD studies of the top two lead molecules, CYP 1A2, ANF, and DBPD, were conducted for 30 ns, which indicated the stability of ANA8430692, followed by ANA7923580. These analogues may potentially serve as potent inhibitors against CYP1A2. Three compounds, namely CHEMBL1, 2, and 3, exhibited superior binding patterns and orientation in the binding pocket of their respective targets, specifically CYP1A1, 1A2, and 1B1, and established strongly bonded and non-bonded molecular interactions, as demonstrated by DBPD and ANF. The designed analogs, specifically ANA6917483, ANA8430692, and ANA6451816, respectively, demonstrated superior binding patterns and orientation in the binding pocket of their respective target proteins, namely CYP1A1, 1A2, and 1B1, and established strong bonded and non-bonded molecular interactions, as demonstrated by DBPD and ANF. Consequently, these compounds may potentially serve as effective anti-cancer agents. However, the stability of the designed leads requires validation through wet-lab experimentation. This study provides significant insights into DBP-mediated mammary cancer and its prevention.

Chapter-1 Introduction and review of literature

1.1 Introduction

Mammary cancer (MC) is the most commonly diagnosed cancer and the primary cause of cancer death in females worldwide. About 85% of malignancy occurs in mammary ducts, and about 15% arises in mammary glandular tissues. Primarily asymptomatic tumor growth is originated in mammary ducts and lobules, having a reduced chance of metastasis. It may spread from surrounding tissues to the breast lymph nodes and other distant body organs as time passes. The latter is the leading cause of the mortality of women worldwide. About 2.3 million individuals suffer from MC, in which more than 6 lakh deaths recorded in 2020. Moreover, about 7.8 million women having MC for the last five years succeeded in their lives by the end of 2020. Compared to other cancers, maximum 'disability-adjusted life years (DALYs)' are seen in the women population suffering from MC, making it one of the most predominant malignancies globally. However, the advancements of sophisticated tools and techniques and systematic implications of early detection programs starting at the beginning of 1980 curtail about 40% of cases by 2020 in socio-economically privileged countries. Although, such countries can drop mortality rates between 2-4% annually. If an annual reduction of 2.5% attains globally, 2.5 million deaths could be curtailed by 2040.[1-5]

MC is a non-communicable disease, and no relation links its progression and development with bacterial and/or viral infection, unlike cervical cancer and human papillomavirus (HPV) infection. There are no substantial risk factors in almost 50% of cases rather than gender and age above 40 years. Major risk factors accountable for MC progression development include family history, obesity, alcohol, overage, prolonged

exposure to radiation and environmental pollution, pregnancy at later age just before the onset of menopause, tobacco smoking, and hormonal therapy after menopause. Avoidance of all lifestyle risk factors can reduce the chance of developing MC up to 30%.[6-8] According to the International Agency for Research on Cancer (IARC), the cases of all types of cancer may be two folds by 2070 in comparison to 2020 if occurrence persists with the current rate especially shown by socio-economic backward countries. If countries fail to implement advanced planning and novel strategies to prevent and control the disease, it may be resulted in an annual increment of 34 million new patients by 2070.[9]

1.1.1 Carcinogens

Cancer-causing agents are generally known as carcinogens. Chemical compounds categorized as a carcinogen does not mean that it will induce cancer. Certain factors cumulatively put the population prone to developing cancer ahead depending on carcinogen exposure and their genetic instability. Carcinogens may increase cancer risk by altering cellular metabolism or damaging DNA directly in cells, which interferes with biological processes, and induces the uncontrolled, malignant division, ultimately leading to tumor formation. Usually, if too severe to repair, DNA damage leads to programmed cell death, but if the programmed cell death pathway is damaged, it cannot prevent itself from becoming a cancer cell.[10] Chemical carcinogens may be genotoxic or nongenotoxic. Genotoxic agents usually refer to carcinogens that either directly bind to or damage genomic DNA, resulting in mutations exerting tumor-promoting activity. Nongenotoxic carcinogens are characterized by promoting activity, hormone modifying, immunosuppressive, cytotoxic, or peroxisome proliferating activity.

1.1.2 Classification of Carcinogen

According to the IARC, chemical compounds have been classified into four groups: Group 1) compounds or mixtures of this group are carcinogenic to humans. The exposure circumstance entails carcinogenic exposures to humans; Group 2A) Compounds or mixtures are probably carcinogenic to humans. The exposure circumstance entails directions that are probably carcinogenic to humans; Group 2B) Chemical agents having minimum possibilities for inducing carcinogenic properties in the human population; Group 3) Compounds or mixtures are not carcinogenic.[11] According to the National Toxicology Program (NTP), the U.S. Department of Health and Human Services categorizes carcinogens into two groups. The first one deals with compounds known as a human carcinogen, and the second one contains chemical agents rationally expected to be a human carcinogen[12]

1.1.3 Dibenzo[*a,l*]pyrene

The scrupulous evidence on dibenzo[*a,l*]pyrene (DBP) and its prevalence to induce cancer have been reported. DBP is a yellow-red odorless crystal classified as group 2A and experimentally estimated human carcinogen by IARC and NTP.[13,14] It is mainly formed due to inefficient combustion of fossil fuels, charcoals, tobacco products, vaping chemicals, woods, plastic wares, and bones. Structurally DBP (CID: 9119) is a six-ringed polycyclic aromatic hydrocarbon and its related fifty-two designated synonyms known in the PubChem database. Structurally DBP shows two grooves, respectively known as bay-and fjord-regions (Figure 1). Intermediates formed due to the latter groove are more susceptible to carcinogenic activities.[15]

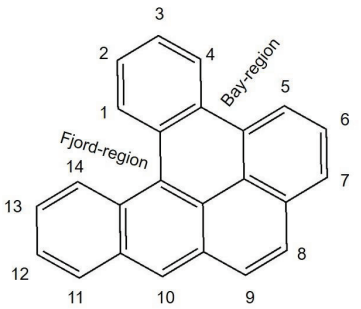

Figure 1.1. Chemical structure of DBP. The numbering shows positions that can form intermediates during bioactivation.

1.2 Review of Literature

1.2.1 Biotransformation of DBP

Genotoxic, mutagenic, and cancer-inducing properties of DBP have been established well by various *in vitro* and *in vivo* experiments. Biotransformation of DBP to DNA-reactive intermediates includes metabolic activation to either diol epoxides through CYP-dependent monooxygenases and epoxide hydrolases or receptive metabolites via an electron oxidation pathway. DBP has been demonstrated to be metabolized by CYP1A1, 1A2, 1B1, 2B6 and 2C9 in cell-free systems and in addition MCF-7 cells to diastereomeric ll,12-diol-13,14-epoxides (Figure 2). DBP is initially oxidized into dibenzo[*a,l*]pyrene-11,12-epoxide using diverse cytochrome CYP450s followed by formation of dibenzo[*a,l*]pyrene-11,12-diol. Further, it is oxidized into an ultimate carcinogenic intermediate dibenzo[*a,l*]pyrene-11,12-diol-13,14-epoxide via numerous CYP450s [17-23].

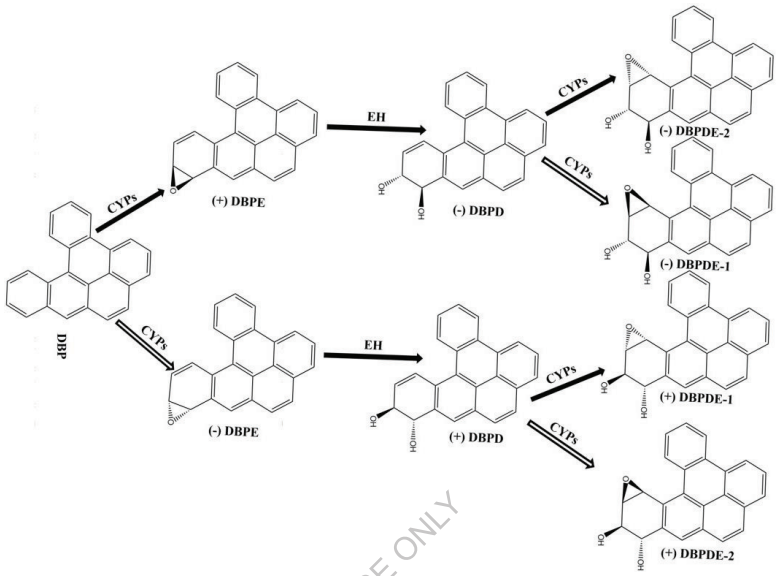

Figure 1.2. Formation and absolute stereochemistry of DBP metabolites responsible for the carcinogenicity of the parent compound. Solid arrows depict the preferred metabolic pathway.

1.2.2 Cytochrome P450 isozymes

CYP450s are major metabolizing enzymes drawing significant consideration by researchers across the globe due to their significant role in the bioactivation of chemical compounds, including environmental pollutants, food additives, drug molecules, mutagens, carcinogens, and adulterants, followed by detoxification via second phase metabolizing enzymes and thus excrete out undesired intermediates formed during metabolic activation of parent compounds. Most of the PAHs produce carcinogenic metabolites upon bioactivation via CYP450s.[24-28] Moreover, almost seventy percent bioactivation of xenobiotics undergoes via CYP450 isozymes (Figure 3).

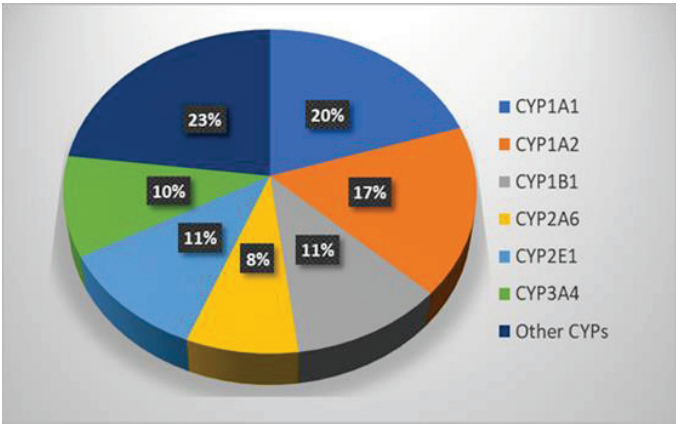

Figure 1.3. Percentage-wise contribution of CYP450s in metabolic bioactivation of PAHs.[28]

Most of the studies reveal that biotransformation of DBP into its carcinogenic metabolite undergo through CYP1A1, 1A2, and 1B1. The cellular fate of DBP as a mammary carcinogen is shown in Figure 4.[15,29,30]

1.2.3 Aryl hydrocarbon receptor-mediated bioactivation

Aryl hydrocarbon receptor (AhR) plays key role in DBP bioactivation akin to other PAHs. Coupling of DBP activates AhR resulting its separation from its complex binding entities e.g., heat shock protein 90, aryl hydrocarbon receptor-interacting protein, and coactivator of Hsp90/70-chaperone system, thereby facilitation of its movement inside the nucleus. Further, the complex AhR-DBP couples to AhR nuclear translocator and thus resulting complex is activated via C-terminus phosphorylation of tyrosine residue. AhR-ARNT complex finds xenobiotic response elements on promoter sites of respective CYP450 isozymes to mitigate their genes. *CYP1A1, 1A2, 1B1* genes are modulated via

the molecular interaction of different coactivators and transcription-regulating factors.[25,31,32]

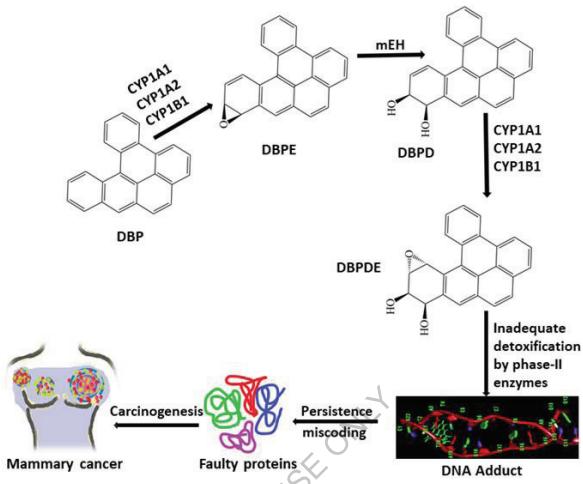

Figure 1.4. The cellular fate of DBP as a mammary carcinogen.[29,30]

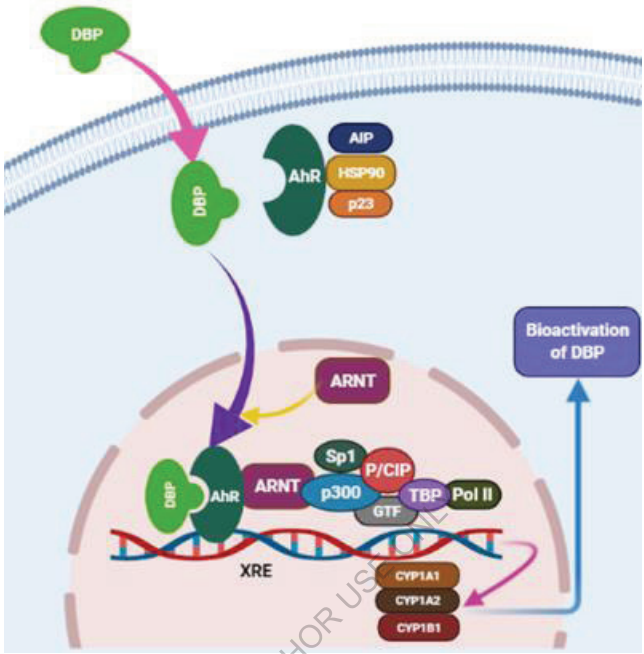

Figure 1.5. AhR-mediated bioactivation of DBP.[25,31,32]

1.2.4 Detoxification of DBP

The balance between the metabolic activation and several detoxification processes influences the intracellular level of diol-epoxide-DNA-adduct formation. Since the sterically hindered bay-region diol-epoxides show an apparent low affinity for microsomal epoxide hydrolase and their half-lives are substantially increased by a stabilization effect of intracellular lipids, the spontaneous and enzymatic catalyzed hydrolysis to less toxic tetraols appear to be of minor importance in the cellular defense against diol-epoxides appear to be the glutathione S-transferase (GST) catalyzed conjugation with glutathione.[33-35]

GSTs are involved in the metabolism of a variety of xenobiotic compounds, including DBP. These enzymes catalyze the conjugation of diverse electrophilic compounds with glutathione, giving rise in most cases to less reactive, water-soluble metabolites that are readily excreted. In humans, four classes of cytosolic GST isozymes (α, μ, π and θ) have thus far been identified, and several of them are polymorphic. Several epidemiological studies have investigated the association of GST genetic polymorphisms with breast cancer risk. Charred meat intake and cigarette smoking are the primary sources of PAH exposure in humans. Some epidemiological studies have suggested that these two lifestyle factors may be associated with the risk of breast cancer.[36-40]

The differences in the activity and enantioselectivity of DBP metabolites depend on their geometry and absolute configuration. For example, the stereoisomeric bay-region diol-epoxides, particularly the syn-diastereomers, were in most cases efficiently conjugated by human GST of class μ (GSTM) wide variations in enantioselectivity ranging from 50-90%. In contrast, human GST of class π showed in most cases only an appreciable activity towards bay-region anti-diol-epoxides and a high preference for conjugation of enantiomers with (R,S,S,R)-configuration.[41-43]

Apart from GST isozymes, another essential phase II enzyme, Arylamine N-acetyltransferase (NAT), plays an essential role in detoxifying heterocyclic amines and other xenobiotics. These cytosolic enzymes are present in eukaryotes and prokaryotes. Humans have two isozymes of arylamine N-acetyltransferases (NAT1 and NAT2) that are 81% homologous but differ in their tissue distribution and substrate specificity. The slow NAT2 acetylation phenotypes have shown a relationship to urinary bladder cancer.

However, NAT polymorphisms linked to colon, breast, lung, and prostate cancers are more controversial.[44-50]

Previous computational study shows the order of binding interaction of GSTP1, GSTM1, and GSTA1 with (-)-*anti*-DBPDE, contrary to the wet-lab findings that emphasized the major enzymatic activity of GSTA1. However, there are no major differences reflected in the above *in silico* findings. It means that (-)-GSTA1, GSTM1, or GSTP1 might conjugate (-)-*anti*-DBPDE. Furthermore, GSTA1, A2, A3, A4, and A5 (A1>A3>A4>A2>A5) also showed plausible binding activity with (-)-*anti*-DBPDE, which is nearly close to experimental data.[51-54] In the case of (+)-*syn*-DBPDE, the binding propensity of GSTM1 was found greater than GSTP1 and GSTA1, which is somewhat similar to the wet-lab findings. Moreover, previous findings exhibited a similar molecular interaction of GSTA1 with both (-)-*anti*-DBPDE and (+)-*syn*-DBPDE. Despite above, molecular interaction of GSTA1, M1 and P1 with (+)-*anti*-DBPDE (GSTA1>M1>P1) and (-)-*syn*-DBPDE (GSTM2>A4>P1) is different and showed comparatively low activity. The binding affinity of NAT2 consistent and greater NAT1 in either (±)-*anti*-DBPDE or (±)-*syn*-DBPDE agreed to the experimental data.[51,52]

1.2.5 DNA adduct formation by diol-epoxides of DBP

DBP diol-epoxides (DBPDEs) form adducts with nucleic acids and proteins via covalent interactions. The adduct formation occurs due to benzylic oxiranyl carbon with exocyclic amino residues dG (deoxyguanosine) and dA (deoxyadenosine). Previous studies show that diol-epoxides of bay regions showing affinity towards N2-amino residue of dG while fjord-region intermediates form N6-amino residue of dA. For example, (+)-anti-BPDE, a bay-region metabolite, exhibits more than ninety percent affinity to form adducts with

dG, while (-)-anti-DBPDE a fjord-region metabolite form more than seventy-five percent adducts with dA adducts. DNA adduct formation with both bay- and fjord-region intermediates is due to their structural variation.[55-64]

DBP diol-epoxide intermediates viz., **(±)**-anti-DBPDE and **(±)**-syn-DBPDE do not form N6-dA adduct. The preferential adduct formation is shown with dT and dG. The cis-and trans- (-)-anti-DBPDE and (+)-syn-DBPDE depicted similar results as above. Structurally the cis-product is less flexible than the trans-intermediates as cis-position shows sterically crowded two hydroxyl groups at the similar site of the benzylic ring while in trans-position, both hydroxy groups located at opposite sides. Diol-epoxide-derived product can be relative to the major or minor groove of DNA helical structure depending upon the structural configuration viz, cis or trans, and dA or dG base preference. Previous *in silico* study shows that N6-dA adduct with trans-(-)-anti-DBPDE, and N6, N7-dA adduct is formed with cis-(-)-anti-DBPDE, trans-(+)-syn-DBPDE, and cis-(+)-syn-DBPDE supporting experimental findings determined so far.[65-71]

Moreover, Ahmad KMK *et al*., 2020 also predicted that the tendency of binding interactions of DBPDEs with DNA is more remarkable than molecular targets of NER pathways concluding that inadequate removal or partial repair of bulky adducts might undergo due to their weak binding forces. The substantial binding of DBPDEs with DNA supports more chemical adduct formation than its removal or repair.[65]

1.2.6 DBP-mediated cell proliferation

Typically, apoptosis occurs via mitochondrial or intrinsic pathway facilitating through proteins of the Bcl-2 family when any gets stressed. Various members of this family having antiapoptotic properties regulates complex programmed cell death

phenomenon.[72-76] The survival or death of a cell depends upon the balance between proapoptotic and antiapoptotic proteins. Dysregulation of BAX or upregulation of Bcl-2 and Bcl-XL hinders apoptosis or vice versa.[77-81] One of the crucial nuclear protein p53 translocate to mitochondria and interacts with antiapoptotic proteins viz., Bcl-2 and Bcl-XL thereby felicitating apoptosis. It may induce programmed cell death by interacting with ARAF1, a key member of apoptosome complex, via activation of Caspase-9. Dysregulation of p53 may hamper the control over cell cycle mechanism, suppressing critical regulators of proapoptotic pathways.[82-89] Deactivation of RB protein leads to the activation and release of E2F, thereby inducing the expression of P14ARF, a negative regulator of MDM2. The MDM2 itself is a negative regulator of p53, inhibition of the former increases the expression of the latter resulting occurrence of programmed cell death.[90-92] Moreover, E2F protein may activate the Bcl-2 and CASPASE family members via cascaded molecular interactions.[93,94]

Moreover, Khan *et al*., 2018 predicted the molecular binding interactions of DBPDEs with CASPASES, BAX, Bcl-2, MDM2, p53, p53-MDM2 complex, p21, p16, CyclinD1-CDK4 complex, CyclinE1-CDK2 complex, H-Ras, K-Ras, BRCA1, and BRCA2. They exhibited the strong binding of Caspase-9 compared to Caspase-8 and Caspase-3 with (-)-*anti*-DBPDE and (+)-*syn*-DBPDE. Caspase-9 and Apaf-1 activate the protease that isolates and activates Caspase-3 and thereby execution of apoptosis. Nevertheless, it may be possible that due to solid interaction, the unavailability of Caspase-9 hampering the reaction with Apaf-1 that may inhibit apoptosis. Further, the strong interaction of DBPDEs with p53 and weak binding with p21, a downstream target of p53 and CDKs inhibitor, p16, a negative regulator of the cell cycle, leads towards suppression of their

expected functionalities. It means that dysregulation of cell cycle checkpoints succeeds towards abnormal cellular proliferation, growth, and development of oncogenic cells.[95]

1.3 Aims and Objectives

For the past few decades, pharmaceutical sectors have been gaining significant attention towards deciphering therapeutically efficacious molecular targets using hybrid approaches of genomics, proteomics, system biology, and traditional experimental biomedical sciences. However, albeit the boom of innovation in high-throughput technology, the functioning of research and development has been honed slowly, resulting in delayed outcomes, especially in drug discovery and development. For example, identifying a new bioactive compound from thousands of lead molecules takes about ten years and costing about $2-3 billion, including bench work to clinical trials, regulatory approval, and delivery to the market. Biomolecular modeling, machine learning, artificial intelligence, and computer-aided drug design (CADD) can speed up the process, reduce surprises and predict the properties, thereby reducing the time and cost of R&D as well. Identifying such therapeutic compounds through virtual screening followed by drug-likeness, ADMET filtration, CYP450 metabolism prediction, and propensities of interaction with other therapeutic molecular targets of biological systems having low toxicity are promising preventive strategies against lifestyle-based diseases. The secret of deciphering novel lead molecules based on their molecular recognition is the ability of one ligand to recognize another. Molecular interactions form the basis of molecular recognition. Biological and cellular functions proceed through various chemical interactions between biomacromolecules and ligands. The efficacy of ligands as an inhibitor is evaluated in terms of ΔG and Ki in CADD. Towards this direction the

prime focus of the current work is to find an effective yet economically sounded novel lead candidates for the prevention and treatment of DBP-mediated mammary cancer using interdisciplinary approaches.

In the proposed work we aimed to identify new therapeutic lead molecules against dibenzo[*a,l*]pyrene-induced mammary cancer using integration of *in silico* and *in vitro* approaches with the following objectives:

- Identification and characterization of drug target (s) involved in dibenzo[*a,l*]pyrene-induced mammary cancer.
- Identification, Design, and optimization of leads, and their molecular interaction study.
- Molecular Dynamics simulation study of potential lead(s).
- *In vitro* validation and explication of best lead.

1.4 Significance

Lead molecules with electron-rich property easily bind with the target proteins and receptors in organisms through non-covalent forces such as van der Waals, electrostatic, hydrogen bonds, coordination bonds and hydrophobic interactions, thereby holding numerous applications in drug discovery. In the proposed work an attempt is made to find novel leads with negligible toxicity by the means of computational design besides searching and identifying anti-cancer agents from existing libraries that can suppress the activity of molecular target (s) involved in DBP-mediated cancer progression directly or indirectly through the integration of of *in silico* and *in vitro* approaches. Further, this work will provide structural insight into the mechanistic details of inhibition of DBP and its metabolites-modulated onset of mammary cancer.

Chapter-2 Computational identification of potential lead molecule(s) against CYP450 1A1, 1A2, and 1B1 isozymes

2.1 Introduction

DBP is one of the deadly pro-carcinogenic environmental polycyclic aromatic hydrocarbons (PAHs) produced by partial oxidation of woods, charcoals, plastic wares, fossil fuels, and tobacco products. It consists of six-fused benzene rings and structurally showing two clefts, respectively known as a fjord- and bay-regions. The former comparatively produces more carcinogenic intermediates.[96-99] Biotransformation of DBP undergoes three consecutive steps. In first step cytochrome P450 (CYP) isozymes especially CYP1A1, 1A2, and 1B1 metabolize DBP into dibenzo[*a,l*]pyrene-11,12-epoxide (DBPE). The second step deals with the microsomal epoxide hydrolase (mEH), which converts DBPE into the dibenzo[*a,l*]pyrene-11,12-dihydrodiol (DBPD). In the final step again CYP isozymes transforms DBPD to its ultimate carcinogenic metabolites dibenzo[*a,l*]pyrene-11,12-dihydrodiol-13,14-epoxide (DBPDE).[100,101] The most potent metabolite DBPDE known among other PAHs reported to date exerts more breast cancer-causing propensities than other human cancers.[102,103]

CYPs have been gaining significant attention from scientists worldwide because of their diverse role in the metabolism of various chemicals, pollutants, food contaminants, drugs, and other xenobiotics, facilitating phase II metabolizing enzymes in their detoxification, thereby preventing undesired effect on human health. However, most PAHs yield reactive carcinogenic metabolites mitigating carcinogenic phenomena upon bioactivation through CYPs. More than 70% biotransformation of PAHs undergo through CYP1A1, 1A2, 1B1, 2A6, 2E1, and 3A4.[103-107] CYPs are heme-containing monooxygenase enzymes representing more than 13,000 and 400 genes under superfamily and family heads across

all the kingdoms known. In humans, about 57 genes and 58 pseudogenes related to various families (18) and subfamilies (44) have been reported.[104] CYPs can be categorized in many ways, CYPs playing a role in detoxification of various chemical compounds, endogenous substance biosynthesis, membrane-attached as in higher organisms, and soluble types as in lower organisms. CYPs of higher organisms found in the endoplasmic reticulum (ER) felicitates via the flavin adenine dinucleotide (FAD) and flavin mononucleotide (FMN) reductase systems. The electron transfer process in prokaryotes and mitochondrial CYPs succeeds through FAD reductase and iron-sulfur cascaded systems. CYPs performing multiple unrelated functions, e.g., biosynthesis of endogenous compounds, are referred to as moonlighting, while those playing a role in xenobiotic metabolism are known as non-moonlighting enzymes.[103,104] The p/CIP and general transcription factors (GTFs) succeed through the interaction of TATA-binding protein (TBP) and RNA polymerase II inducing CYPs enzymes, which later metabolize DBP into its most hazardous carcinogenic intermediate DBPDE.[104,108,109]

Bioactivation of DBP occurs through coupling with the aryl hydrocarbon receptor (AhR), as happens in most PAHs, including the prototype PAH benzo[*a*]pyrene (BP). Upon DBP binding, the AhR detaches from its complex regulating and activating partners viz., aryl hydrocarbon receptor-interacting protein (AIP), heat shock protein 90 (Hsp90), and p23 (coactivator of Hsp90/70- chaperone system) and moves to the nucleus. The DBP-AhR complex binds with AhR nuclear translocator (ARNT). The DBP-AhR-ARNT complex activates through the phosphorylation of tyrosine amino acids at the C-terminus of AhR. Further, AhR-ARNT identifies xenobiotic response elements (XREs) on their respective CYPs promoter sites to modulate their genes. The genes for CYP1A1, 1A2, 1B1 enzymes

mitigate through the molecular interaction of various coactivators and transcription-regulating factors viz., specificity protein 1 (Sp1), p300, co-integrator-associated protein

The study aims to inhibit CYP1A1, 1A2, and 1B1 by novel lead molecules, thereby preventing carcinogenic DBPDE -induced mammary cancer. Alpha-naphthoflavone (ANF), a known inhibitor of selected CYPs, was used as a template to find out potential lead molecules using integrated computational and bioinformatics approaches viz., high-throughput ligand-based virtual screening (LBVS), drug-likeness filtration, docking studies, and MD simulations (MDS). Post docking analysis of top hits, dynamics simulation, and their comparison with known inhibitor ANF yield one of the best lead molecules. The study's findings uncover substantial mechanistic insight into the targeted therapy and prevention of PAH-induced mammary malignancies.

2. 2 Materials and Methods

2.2.1 CYP isozymes 3D structure retrieval

The 3D crystal structure of CYP1A1 (4I8V), CYP1A2 (2HI4), and CYP1B1 (3PM0) complexed with ANF (CID: 11790) retrieved from research collaboratory for structural bioinformatics (RCSB) protein data bank (PDB) (https://www.rcsb.org/). ANF ligand truncated from the complex and apoprotein, and heme group considered to make input files compatible for molecular interactions via truncating unwanted heteroatoms, ions, and molecules. The 3D coordinates of co-complexed ANF carried forward to study identified new chemical molecules. The relevant force field and energy optimization algorithm was employed to get proteins energetically minimized and optimized.[110,111]

2.2.2 Virtual screening, ADMET analysis, and optimization

The hybrid technique, including molecular fingerprints, electro shape, spectrophores, shape IT, and align IT of LBVS approach searched various hits akin to the ANF molecule from publicly available virtual databases viz., DrugBank, ChEMBL of EMBL-EBI, Chemical Entities of Biological Interest (ChEBI) database, GPCR-Ligand Association (GLASS) database, Human Metabolome Database (HMDB), and ZINC database.[112,113] The identified ligands were tested on Lipinski rule of five (RO5) (Molecular weight <=500 Da; HBD <=5; HBA<=10; LogP <= 5). The RO5-satisfied ligands sifted through absorption, distribution, metabolism, elimination, and toxicity (ADMET) descriptors using the PreADMET server.[114-117] Ligands succeeded ADMET descriptors were prepared for molecular interaction studies by assigning suitable energy minimization and optimization algorithms.[110,111]

2.2.3 Molecular docking

Molecular interaction of selected ligands with CYP isozymes carried out using AutoDock Tools 4.0 (ADT) to get plausible binding mode. Four input files viz., pdbqt files of both ligand and protein, grid parameter file, and docking parameter file prepared to execute ADT. The grid was generated in such a way so that the ligand gets enough space to move within it freely. 62 Å grid points separated each x, y, z axes, and spacing between the two grids set at 0.92 Å. Twenty runs for each ligand molecule employed in ADT. Post docking analysis depicted one of the ligand's best conformations with minimum binding energy (ΔG) carried forward for further molecular simulation analysis.[118-120]

2.2.4 MD simulation

MDS of 50 ns was employed to assess the flexibility and stability of CHEMBL1, 2, and 3 with CYP1A1, 1A2, and 1B1 enzyme respectively at 300 K using Groningen Machine for Chemical Simulations (GROMACS) package. The PRODRG server was used to generate topology and force-field parameter (ffp) files of all ligands. CYP1A1-ANF, CYP1A2-ANF, CYP1B1-ANF, CYP1A1-CHEMBL1, CYP1A2-CHEMBL2, and CYP1B1-CHEMBL3 complexes were absorbed in an orthorhombic water box at 10 Å edge settings. The Na+ and Cl- ions were added as a neutralizing agent and to preserve 0.15 M physiologic concentration. The prepared system was energetically minimized at 2000 steps using the steepest descent algorithm. Two phases viz., NVT (constant number of particles, volume, and temperature) and NPT (constant number of particles, pressure, and temperature) ensembles were utilized to achieve the equilibration process. Post equilibration, the smooth particle-mesh-Ewald technique was used, followed by the execution of production phases of 50 ns duration. Analysis of all trajectories was accomplished through different GROMACS command utilities.[121-123] The flow chart of the adopted methodology is shown in Figure 2.1.

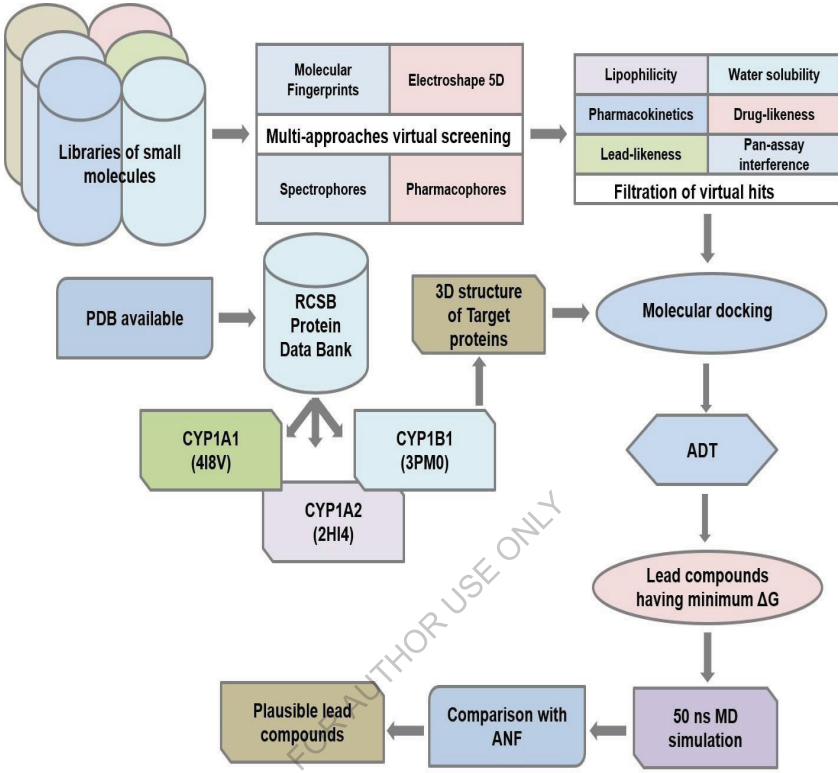

Figure 2.1. Flow chart of the adopted methodology.

2.3 Results and Discussion

2.3.1 Drug-likeness and ADMET filtration.

LBVS predicted 38,000 chemical hits out of 11,175,625 compounds of various virtual libraries of the Swiss Similarity database.[113] The RO5 filtration yielded 38,000 molecules, in which 400 molecules succeeded for HIA (human intestinal absorption; activity range: poorly- 0~20%, moderate- 20~70%, high- 70~100%), BBB (blood-brain barrier; CNS active compounds (+): >1, CNS inactive compounds (-): <1), PPB (plasma protein binding; chemicals strongly bound > 90%, chemicals weakly bound < 90%),

MDCK (Madin-Darby canine kidney; lower-< 25, moderate-5~500, Higher- > 500) cell permeability, heterogeneous human epithelial Caco2 cell permeability (lower-<4, moderate-4~70, higher->70), and mutagenicity and carcinogenicity rat and mouse models filtering non-toxic compounds as ADMET descriptors.[125]

2.3.2. Molecular docking and MD simulation.

ADMET-satisfied 400 compounds akin to the ANF were subjected to dock with each CYP1A1, 1A2, and 1B1 predicting the most probable binding interactions. DBPD and ANF exhibited ΔG values of -7.12 kcal/mol, and -9.13 kcal/mol with CYP1A1, -9.93 kcal/mol, and -9.66 kcal/mol with CYP1A2, -10.08 kcal/mol, -9.67 kcal/mol with CYP1B1 respectively. Respectively, 83, 32, and 30 ligands comparatively depicted better interactions in terms of free energy of binding ΔG (kcal/mol) with CYP1A1, 1A2, and 1B1. Docking analysis of the top 10 ligands with each CYP isozyme is shown in Table 2.1, 2.2, and 2.3.

Table 2.1. Molecular interactions of top 10 ligands, ANF, and DBPD with CYP1A1.

S. No.	Ligands	ADT (ΔG)	H-bonds
01.	CHEMBL224064	-10.52	V387- HN…O12-LIG, R396-HE…O12-LIG
02.	CHEMBL2420082	-09.99	S87- HG…O-LIG
03.	CHEMBL2420083	-10.46	S87- HG…O-LIG
04.	CHEMBL2420094	-10.35	S87- HG…O-LIG
05.	CHEMBL2420096	-10.04	D285- OD1…H-LIG
06.	CHEMBL2420099	-09.85	S87- HG…O-LIG
07.	CHEMBL2431801	-09.99	S87- HG…O-LIG
08.	CHEMBL595616	-10.28	D285- OD1…H-LIG, I414- O…H-LIG
09.	CHEMBL595631	-10.12	W96- HE1…N-LIG, R420- HH11…N-LIG

10.	CHEMBL487213	-09.87	S87- HG…O-LIG
11.	ANF	-09.13	Nil
12.	DBPD	-07.12	V453-NH…O2-LIG

Table 2.2. Molecular interactions of top 10 ligands, ANF, and DBPD with CYP1A2.

S. No.	Ligands	ADT (ΔG)	H-bonds
01.	CHEMBL2420091	-10.45	R75-HH12…O-LIG
02.	CHEMBL2420094	-10.58	R219-HH12…O-LIG
03.	CHEMBL595616	-10.73	R423-O…H-LIG, D287-OD1…H-LIG
04.	CHEMBL2331821	-10.42	R75-HH12…O-LIG
05.	CHEMBL2420097	-10.65	R75-HH12…O-LIG
06.	CHEMBL2431801	-10.48	R75-HH12…O-LIG
07.	CHEMBL2420083	-10.82	G14-NH…O5-LIG
08.	CHEMBL2420100	-10.76	N157-HD2…O-LIG, R219-HH21…O-LIG
09.	CHEMBL127267	-10.57	I353-H…N-LIG
10.	CHEMBL2431819	-10.52	I426-H…O-LIG
11.	ANF	-09.66	R263-NH…O1-LIG
12.	DBPD	-09.93	A102-O…H42-LIG

Table 2.3. Molecular interactions of top 10 ligands, ANF, and DBPD with CYP1B1.

S. No.	Ligands	ADT (ΔG)	H-bonds
01.	CHEMBL61745	-10.81	N353-HE2…F-LIG
02.	CHEMBL241830	-10.44	E162-H…O-LIG
03.	CHEMBL2420091	-10.46	R50-HH12…O2-LIG, I391-O…H-LIG
04.	CHEMBL2420099	-10.51	D262-OD2…H-LIG
05.	CHEMBL595616	-10.55	D262-OD2…H-LIG
06.	CHEMBL595631	-10.68	D262-OD2…H-LIG

S. No.	Ligands	ADT (ΔG)	H-bonds
07.	CHEMBL2420097	-10.63	D262-OD2…H-LIG
08.	CHEMBL2393069	-10.78	D255-OD2…H-LIG
09.	CHEMBL595407	-10.58	I391-O…H-LIG
10.	CHEMBL288714	-10.55	K383-HZ1…N-LIG
11.	ANF	-09.67	R373-HH12…O2-LIG
12.	DBPD	-10.08	W354-HE1…O2-LIG

Ligands tabulated showing a more significant binding affinity than the ANF and DBPD with their respective CYP1A1, 1A2, and 1B1 isozymes. Among all ligands, CHEMBL224064 (CHEMBL1) exhibited better interaction with CYP1A1 (ΔG: -10.52 kcal/mol) along with two H-bonds (V387-HN…O12-LIG, R396-HE…O12-LIG), supporting the stability of the docked molecule. The detailed molecular interactions of CHEMBL1, ANF, and DBPD with CYP1A1 are illustrated in Ligplot[126] (Figure 2.2).

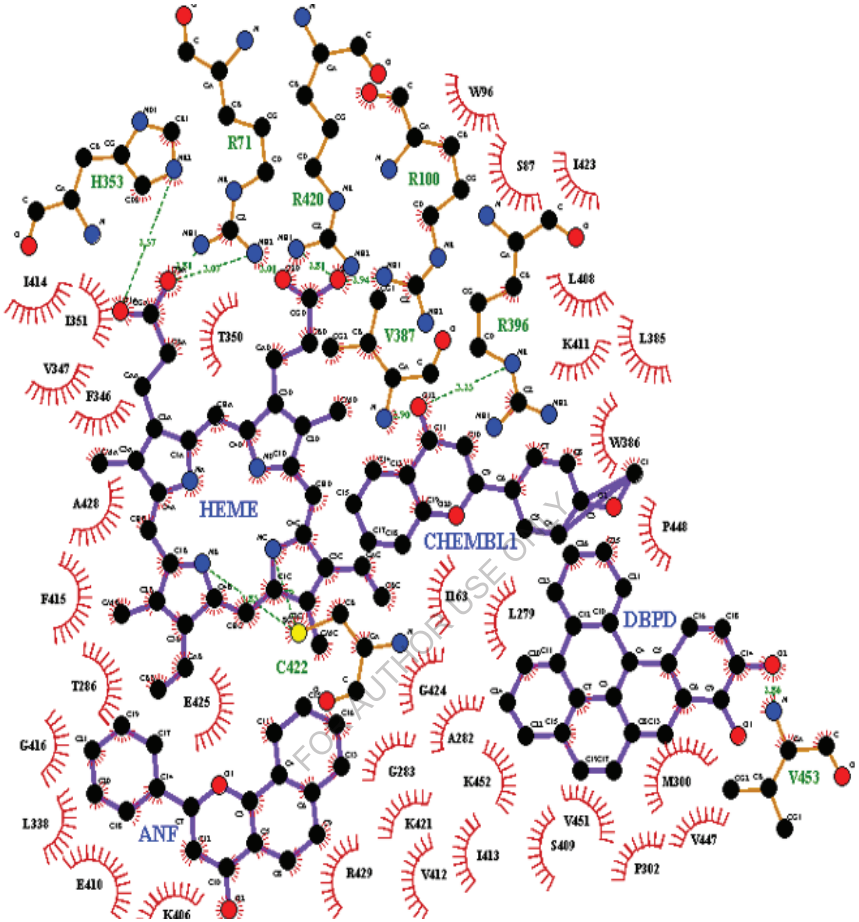

Figure 2.2. The 2D Ligplot of CYP1A1 with CHEMBL1, DBPD, and ANF. Dashed lines (green) and arcs, respectively, represent H-bonds and hydrophobic contacts.

CHEMBL1 is also found closer to the heme group in comparison to DBPD and ANF. DBPD forms one H bond (V453-NH…O2-LIG), while hydrophobic residues are in close contact with ANF without any H-bond. Likewise, CHEMBL2 displayed strong

interaction with CYP1A2 (ΔG: -10.82 kcal/mol) with one H-bond (G14-NH…O5-LIG), making the docked complex stable. Moreover, it is also fitted to the cleft of heme compared to DBPD and ANF. One H-bond is also formed by each DBPD (A102-O…H42-LIG) and ANF (R263-NH…O1-LIG). The detailed illustration of CHEMBL2, DBPD, and ANF with CYP1A2 is given in Figure 2.3.

Similar to the CHEMBL1 and 2, CHEMBL3 interacted more efficiently to CYP1B1 (ΔG: -10.81 kcal/mol), rendering the docked complex stable with one H-bond (N353-HE2…F-LIG) formation. Additionally, it is also anchored near to heme, unlike DBPD and ANF. W354 and R263 form H-bond with respectively second and first oxygen of DBPD and ANF. Ten amino acid residues of CYP1B1, namely- arginine50, methionine65, threonine327, isoleucine328, glutamine353, isoleucine391, serine393, arginine397, cysteine399, and isoleucine400, exhibited significant interactions with both ligand CHEMBL3 and heme-conjugated ring system. The detailed molecular interaction of CHEMBL3, DBPD, and ANF with CYP1B1 is exemplified in Figure 2.4.

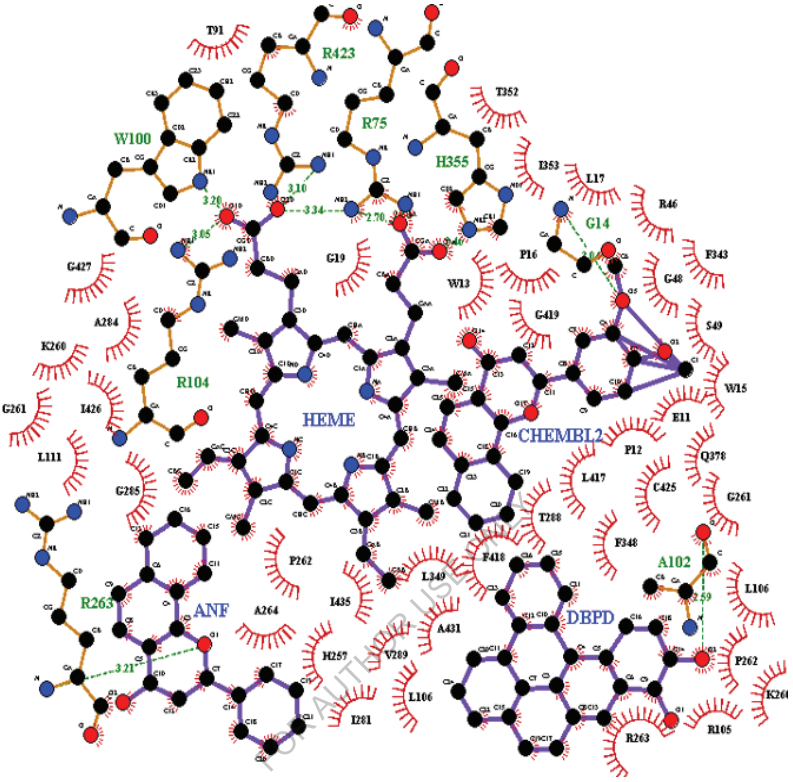

Figure 2.3. The 2D Ligplot of CYP1A2 with CHEMBL2, DBPD, and ANF. Dashed lines (green) and arcs, respectively, represent H-bonds and hydrophobic contacts.

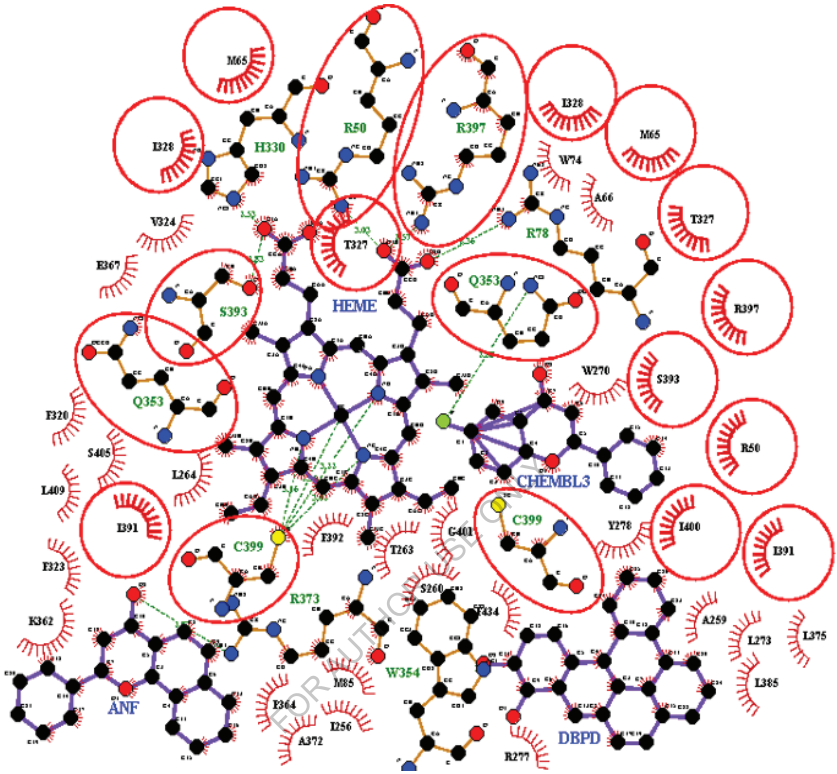

Figure 2.4. The 2D Ligplot of CYP1B1 with CHEMBL3, DBPD, and ANF. Dashed lines (green) and arcs, respectively, represent H-bonds and hydrophobic contacts. Encircled residues are showing common interactions with the heme-conjugated ring system and ligand CHEMBL3.

Most of the residues of CYP1B1 are showing similar interactions with its heme group and CHEMBL3, along with the substantial free energy of binding (ΔG: -10.81 kcal/mol). CHEMBL2393069 also exhibited strong interaction having -10.78 kcal/mol free energy of binding along with one H-bond formation (D255-OD2…H-LIG). Therefore, 50 ns

MDS for the complexes CYP1B1-CHEMBL3, CHEMBL2393069, DBPD, and known inhibitor ANF were executed to foresee the stability of docked molecules. The root-mean-square deviation (RMSD) plot showcases ligands-protein docked complexes' stability.[127] The RMSD graph reveals that the CYP1B1-CHEMBL3 complex is in a more stable form, followed by CHEMBL2393069, ANF, and DBPD. The root-mean-square fluctuation (RMSF) aims to determine the stability of complexes during the entire time-scale of MDS.[128] The solvent-accessible surface area (SASA) exposes the target protein's surface area accessible by the solvent molecule.[129] The RMSD, RMSF, and SASA plots favor the CYP1B1-CHEMBL3 complex's stability compared to CHEMBL2393069, DBPD, and ANF (Figure 2.5, 2.6, and 2.7).

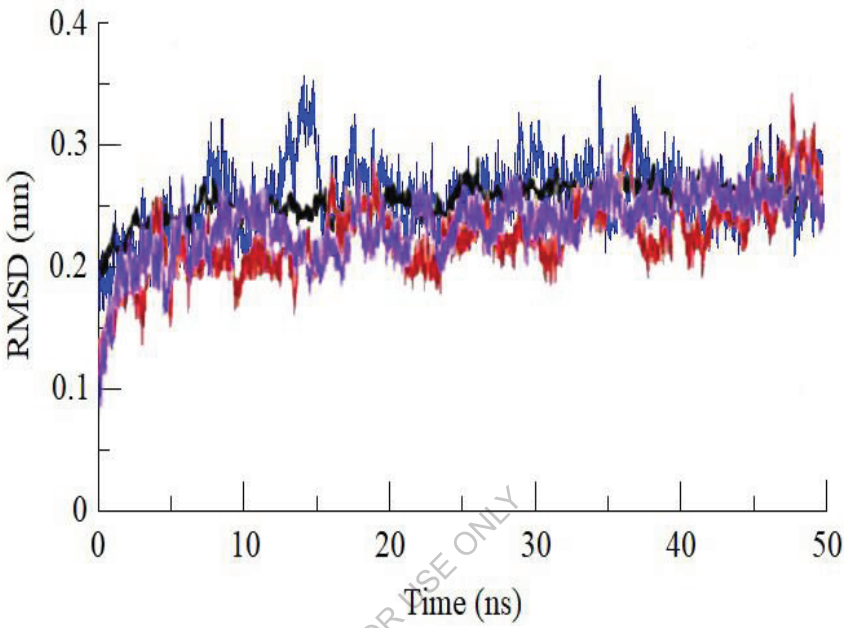

Figure 2.5. MD simulation of ligands binding to the CYP1B1. RMSD plot as a function of time. Magenta, red, blue, and black colors represent CHEMBL3, CHEMBL2393069, DBPD, and ANF, respectively.

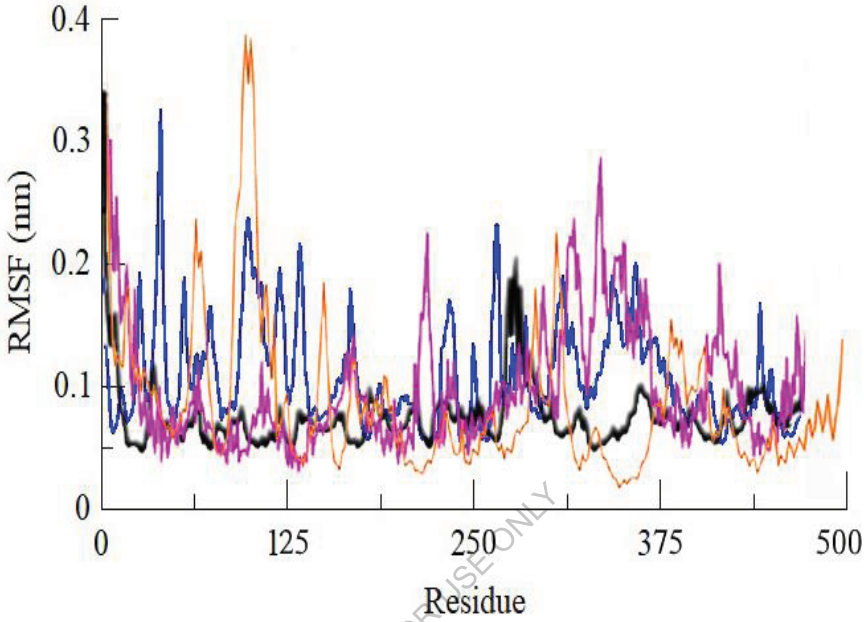

Figure 2.6. MD simulation of ligands binding to the CYP1B1. RMSF plot for CHEMBL3 (pink), CHEMBL2393069 (saffron), DBPD (blue), and ANF (black) respectively.

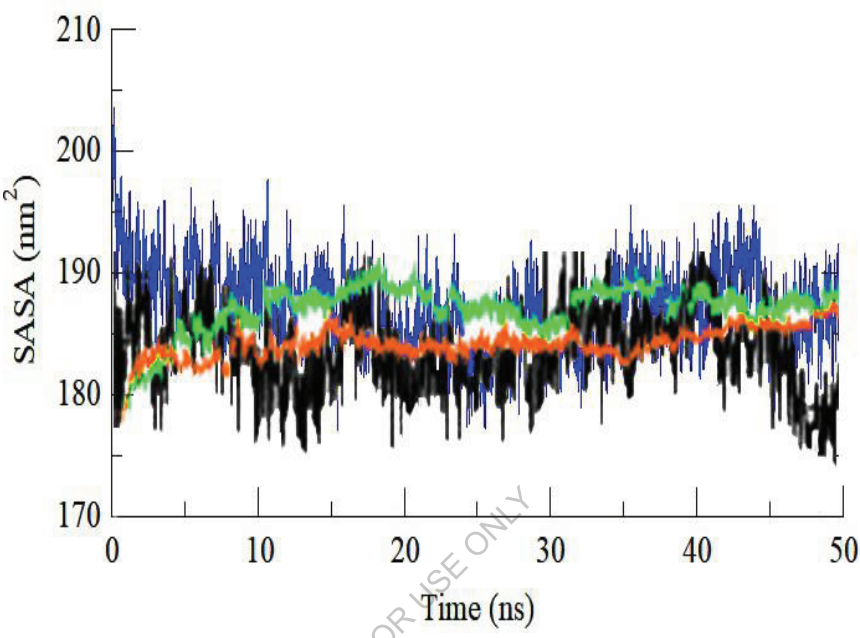

Figure 2.7. MD simulation of ligands binding to the CYP1B1. SASA plot for CHEMBL3 (green), CHEMBL2393069 (saffron), DBPD (blue), and ANF (black) respectively.

2.4. Conclusions

AhR and its other associated proteins facilitate the biotransformation of DBP, as shown in Figure 2.3. CHEMBL1 (6-iodo-4'-methoxyflavone), CHEMBL2 (3',4'-dimethoxy-alpha-naphthoflavone), and CHEMBL3 (6-fluoroflavone) exhibited better molecular interactions with CYP1A1, CYP1A2, and CYP1B1, respectively, as shown by *in silico* findings viz., molecular docking and MD simulation analysis. These compounds were found docked into the binding pocket of their respective targets with excellent binding pattern and orientation, thereby establishing strong bonded and non-bonded molecular interactions compared to DBPD and ANF. The proximity of lead molecules

near the heme-ring system's cleft might disturb the consensus motif signature of selected metabolizing enzymes, thus inhibiting the formation of carcinogenic metabolites. Moreover, these compounds having significant inhibition properties might be used as promising lead molecules against CYP1A1, 1A2, and 1B1 isozymes.

Chapter-3 Combinatorial design to identify potential inhibitor(s) against CYP450 1A1, 1A2, and 1B1 isozymes

3.1 Introduction

A series of catalytic reactions facilitate the biotransformation of DBP into its carcinogenic diol-epoxides (DEs). The majority of diol-epoxide-derived DNA adducts have been found to result from the reaction of the benzylic oxiranyl carbon of the molecule with the exocyclic amino groups of the DNA bases dG and dA.[129-133] The adducts of DNA show that bay-region DEs like to form chemical adducts at the N2-amino group of dG, while sterically hindered fjord-region DEs favours the reaction N6-amino group of dA. For instance, the bay-region diol-epoxide (+)-anti-benzo[*a*]pyrene-7,8-diol-9,10-epoxide (BPDE) has >90 % preference of forming DNA adducts with dG whereas fjord region diol-epoxide (-)-anti-DBPDE exhibits more than 70% adducts for dA.[134-137] The differences may be due to their structural distortions.[138,139]

DNA damage that may emerge in a cell, flexible and complex cell apparatus contained a few distinct pathways have been well studied.[140-142] The two main mechanisms for DNA repair are BER and NER pathways. The clearest capacity of NER in an individual is to eliminate those photoproducts from DNA brought about by UV radiation. It is self-evident in people with NER deserts, e.g., xeroderma pigmentosum (XP), where patients show a high rate of UV-related skin diseases. Be that as it may, NER has additionally been demonstrated to be an effective DNA repair mechanism for wiping out countless massive adducts of PAHs.[143-145]

In normal cells, stress starts apoptosis through the mitochondrial or intrinsic pathway, and the Bcl-2 family proteins assume a fundamental part in the apoptotic reaction. These

proteins are described by the presence of 1-4 saved Bcl-2 homology (BH) domain. The Bcl-2 family has several antiapoptotic proteins that directly influence the permeability of the mitochondrial membrane to regulate apoptosis. The interaction of BAX with the mitochondrial membrane causes cytochrome *c*, which binds to apoptotic-releasing factor 1in the cytosol. The limiting outcomes in the enactment of cysteine-aspartic corrosive protease-9 (Caspase-9) are needed to frame the apoptosome complex to start apoptosis. The apoptotic reaction is fundamentally reliant upon the proportion of the outflow of proapoptotic and antiapoptotic Bcl-2 individuals.[146-150]. An absence of BAX or an increment of Bcl-2 or Bcl-XL smothers apoptosis, while a decline of Bcl-XL or Bcl-2 upgrades apoptosis. Dimers containing BAX and Bcl-2 inactivate BAX, thereby inhibiting the apoptosis.[151-152]

The p53 is an essential protein. It might work outside the core by moving to the mitochondria, where it associates straightforwardly with antiapoptotic proteins, for example, Bcl-2 and Bcl-XL, to initiate apoptosis. Further, in addition to having direct effects on Bcl-2 family proteins, the p53 protein also increases the activity of *the APAF1* gene, a member of the apoptosome complex, and is critical for the activation of Caspase-9 to initiate apoptosis. On the other hand, the inactivation of p53 leads to a deregulation of cell-cycle control and a suppression of many crucial proapoptotic pathways. The subsequent loss of p53 function markedly decreases the sensitivity of lung cancer cells to apoptosis induced by exposure to tobacco smoke or other stresses.[153]

Computational data reported so far uncovers the preferable molecular interactions of different diol-epoxides of DBP and BP with caspases-3, 8, 9, BAX, Bcl-2, MDM2, p53, p53-MDM2 complex, p21, p16, CyclinD1-CDK4 complex, CyclinE1-CDK2 complex,

H-Ras, K-Ras, BRCA1 and BRCA2. The findings exhibit more involvement of caspase-9 than caspase-8 and caspase-3 towards the interactions with potent carcinogenic metabolite, (-)-*anti*-DBPDE, (+)-*syn*-DBPDE of DBP, and (+)-*anti*-BPDE of BP favours the participation of caspase-9 in the activation cascade of other caspases. The Apaf-1 and Caspase-9 complex leads to activation of the protease, thereby cleaving and activating caspase-3 responsible for apoptosis execution. However, due to tight binding between metabolites and protein, caspase-9 might be no longer available for reaction with Apaf-1, which may inhibit apoptosis.

Further, stronger interactions of diol-epoxides of DBP and BP with p53, weak interactions with p21 (a downstream target of p53 and a CDK inhibitor), and p16 (a negative regulator of the cell cycle) exhibited the suppression of their normal function, i.e., no proper regulation of cell cycle checkpoints resulting in the proliferation of cells containing genetic instability. In addition, DBP diol-epoxides strongly interacted with both oncoproteins H-Ras and K-Ras and tumor suppressor proteins BRCA1 and BRCA2 suggesting to be comparatively more substantial mammary carcinogen than BP showed weak interactions with BRCA1 and BRCA2 while exhibiting higher interactions with H- and K-Ras.[17,54,64,95]

In the proposed work in silico approach was used to identify potent inhibitors of CYP450 1A1, 1A2, and 1B1 alpha-naphthoflavone (ANF), a known inhibitor was used to understand the molecular recognition interactions using molecular docking and molecular dynamics analysis. A side chain or moiety replacement transforms an active compound into another compound that shares similar shapes, volumes, electronic distributions, and physicochemical properties, which produce similar biological properties. Scaffold

replacement is widely used in drug discovery to improve potency and selectivity, solve problems associated with drug pharmacokinetics, and remove unwanted side effects such as toxicity and metabolic liabilities.[154]

ANF was selected as a template for combinatorial design and 400 analogs designed by combinatorial chemistry tool. The top rank hits were further subjected to drug-likeness prediction filters and found analog 300 out of 400. The second filter was ADMET prediction, in which 100 analogs were found. After comparison with DBPD and ANF, 80 hits succeed for molecular docking. MD simulation study of the top two lead molecules was performed and compared with DBPD and ANF. Post MD simulation analysis predicts one of the best leads that may be useful as an inhibitor molecule against CYP1A1.

3.2 Materials and Methods

3.2.1 3D structure retrieval and preparation of proteins

The retrieval, optimization, and energy minimization of selected proteins were accomplished as mentioned in section 2.2.1.[110,111]

3.2.2 Combinatorial design of ANF analogues

ANF is the known inhibitor of CYP450 1A1, 1A2, and 1B1. Four hundred compounds akin to ANF were designed using combinatorial chemistry modules of VLife's Aakar tool. Optimization and energy minimization of all designed analogues was carried out using the same procedures as adopted in section 2.2.2.[110,111]

3.2.3 Drug-likeness and ADMET prediction

Prediction of Lipinski RO5 and ADMET filtrations was made using the same methodology as used in section 2.2.2.[114-117]

3.2.4 Docking simulations

Polar H-atoms, Kollman united atom, and atom type parameters were added, and further, non-polar H-atoms were merged during the generation of the protein pdbqt file. During the ligand pdbqt file preparation, polar H-atoms were added, non-polar H-atoms merged, number of torsions and rotatable bonds were defined. The cubic volume of 65 × 65 × 65Å with 0.678Å grid points spacing and center coordinates was set according to the surface of the protein, providing ample space for movement of ligands. The remaining procedures were similar as discussed in section 2.2.3.[118-120] The adopted methodology is summarized in Figure 3.1.

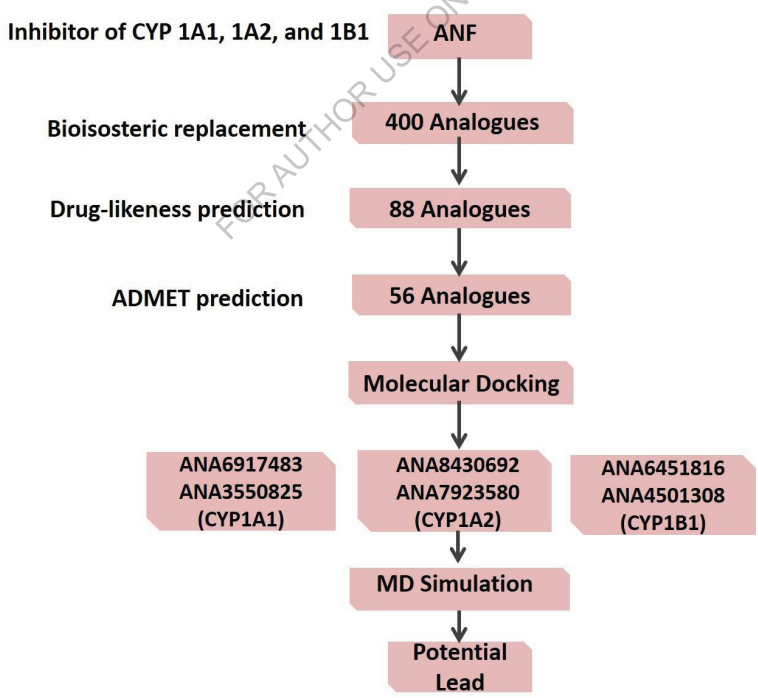

Figure 3.1. Flow chart of the adopted methodology.

3.3 Results and Discussion

The combinatorial approaches were implemented to design and depict the most probable inhibitor molecules against selected CYP450 isozymes. Using ANF as a template, four hundred analogues were designed, followed by lead-like and ADMET filtration.

3.3.1 Lipinski RO5 filtration

Analogues obeyed 3 out of 4 rules of RO5 were taken forward for ADMET filtration. RO5 filtered compounds are listed in Table 3.1.

Table 3.1. List of analogues obeyed Lipinski RO5 filtration.

S. No.	Analogues	MW (g/m)	HBD	HBA	LogP
1.	ANA1145706	224.08	0	2	3.51
2.	ANA1222005	273.08	0	3	4.01
3.	ANA1432644	286.10	0	2	4.54
4.	ANA1447285	278.04	0	2	4.68
5.	ANA1459513	252.12	0	2	4.24
6.	ANA1546568	238.10	0	2	3.90
7.	ANA1573680	340.01	0	2	5.92
8.	ANA1630064	322.10	0	2	5.77
9.	ANA1631036	262.06	0	3	4.21
10.	ANA1818035	226.06	0	3	2.96
11.	ANA2049747.	322.10	0	2	5.77
12.	ANA2113872	252.12	0	2	4.29
13.	ANA2222312	264.12	0	2	4.60
14.	ANA2361823	264.04	0	2	3.97
15.	ANA2419400	340.01	0	2	5.92
16.	ANA2457386	222.07	0	2	3.59
17.	ANA2522095	316.07	0	2	4.34

18.	ANA2685819	278.04	0	2	4.68
19.	ANA2992179	290.07	0	2	4.75
20.	ANA2998544	221.05	0	3	2.82
21.	ANA3127481	308.07	0	3	4.89
22.	ANA3181590	240.04	1	4	2.64
23.	ANA3212034	286.10	0	2	4.92
24.	ANA3421779	340.01	0	2	5.92
25.	ANA3484613	266.13	0	2	4.68
26.	ANA3517652	241.04	0	5	2.85
27.	ANA3544010	250.10	0	2	4.21
28.	ANA3550825	311.10	1	3	5.10
29.	ANA3751883	308.07	0	2	4.89
30.	ANA3789084	240.08	1	3	2.48
31.	ANA4037701	262.06	0	3	4.21
32.	ANA4329694	304.07	2	4	4.02
33.	ANA4476929	306.05	0	2	5.27
34.	ANA4501308	332.11	0	4	4.63
35.	ANA4550544	268.07	0	4	3.12
36.	ANA4584630	308.07	0	2	4.89
37.	ANA4604071	279.04	0	3	4.07
38.	ANA4617085	300.12	0	2	5.23
39.	ANA4632578	239.10	0	3	3.01
40.	ANA4637969	306.05	0	2	5.27
41.	ANA4741385	254.06	0	4	2.73
42.	ANA4835276	340.01	0	2	5.92
43.	ANA4891873	236.08	0	2	3.68
44.	ANA5085235	281.11	0	4	2.78
45.	ANA5201204	318.09	1	4	4.33
46.	ANA5259689	302.09	0	3	4.62
47.	ANA5588223	330.16	0	2	5.41

48.	ANA5634920	239.06	2	4	2.05
49.	ANA5635542	300.12	0	2	5.23
50.	ANA5729459	220.05	0	2	2.93
51.	ANA5923031	300.12	0	2	5.23
52.	ANA5998351	286.10	0	2	4.92
53.	ANA6026462	274.07	0	4	3.40
54.	ANA6051968	290.07	0	2	4.75
55.	ANA6055150	292.15	0	2	5.38
56.	ANA6069175	286.10	0	2	4.92
57.	ANA6115436	226.06	1	3	2.44
58.	ANA6263440	280.11	0	3	3.84
59.	ANA6451816	302.09	0	3	4.62
60.	ANA6505199	324.04	0	2	5.41
61.	ANA6550068	252.12	0	2	4.46
62.	ANA6917483	274.07	0	4	3.40
63.	ANA6928213	290.07	0	2	4.75
64.	ANA6973880	242.04	0	2	3.67
65.	ANA7055846	240.08	0	3	3.35
66.	ANA7113102	340.07	0	2	5.63
67.	ANA7145504	288.08	1	3	4.32
68.	ANA7192589	349.99	0	2	5.38
69.	ANA7296445	250.10	0	2	3.90
70.	ANA7325519	238.06	0	3	3.15
71.	ANA7438000	300.12	0	2	5.23
72.	ANA7451007	279.13	0	3	3.94
73.	ANA7481255	276.08	0	3	4.13
74.	ANA7527053	300.12	0	2	5.23
75.	ANA7609797	280.04	0	3	3.85
76.	ANA7923580	308.07	0	2	4.89
77.	ANA7963753	408.06	0	2	6.65

78.	ANA7993024	266.13	0	2	4.54
79.	ANA8002870	287.10	0	3	3.93
80.	ANA8321607	274.07	0	4	3.40
81.	ANA8430171	265.11	0	3	3.55
82.	ANA8430692	266.13	0	2	4.85
83.	ANA8450389	254.09	0	3	3.14
84.	ANA8539067	323.10	0	3	5.16
85.	ANA8583069	287.10	0	3	3.93
86.	ANA8871618	287.10	0	3	3.93
87.	ANA8886081	253.07	1	4	2.91
88.	ANA8969446	250.10	0	2	4.37

3.3.2 ADMET filtration

RO5-satisfied analogues were passed through different ADMET parameters. Analogues showing their values in the specified range of ADMET descriptors are listed in Table 3.2.

Table 3.2. ADMET filtration.

S. No.	Analogues	#HIA	$BBB	@PPB	&MDCK cell permeability	*CaCo2 cell permeability	Ames test	Mouse Model	Rat Model
1.	ANA1222005	100.00	1.11	100.00	19.45	52.40	NM	P	P
2.	ANA1447285	100.00	1.81	100.00	22.67	56.27	NM	P	N
3.	ANA1459513	100.00	0.45	100.00	0.09	46.45	NM	P	P
4.	ANA-1546568	97.91	2.26	90.20	254.47	1.83	NM	N	P
5.	ANA1630064	100.00	1.87	98.43	29.37	54.16	NM	P	P
6.	ANA1631036	98.57	1.24	91.36	353.32	0.35	NM	P	P
7.	ANA1818035	100.00	1.36	96.34	16.06	57.02	NM	P	N
8.	ANA2049747	100.00	1.40	93.95	27.71	56.57	NM	N	N
9.	ANA2113872	96.22	0.10	93.95	19.17	38.86	NM	N	P
10.	ANA2361823	100.00	1.98	99.30	32.16	47.59	NM	P	N
11.	ANA2419400	100.00	1.51	95.36	37.37	55.46	NM	P	N

12.	ANA2457386	100.00	0.99	94.58	47.91	57.05	NM	N	N
13.	ANA2998544	100.00	2.19	93.96	44.90	56.92	NM	N	N
14.	ANA3127481	95.55	0.84	83.88	50.71	13.40	NM	N	P
15.	ANA3181590	100.00	1.70	93.89	15.91	56.56	NM	N	N
16.	ANA3212034	100.00	1.68	99.75	16.83	52.40	NM	P	P
17.	ANA3484613	98.43	1.65	94.86	12.03	53.13	NM	N	N
18.	ANA3544010	100.00	0.61	93.85	15.98	56.24	NM	N	N
19.	ANA3550825	100.00	1.43	99.04	37.46	56.20	NM	N	N
20.	ANA4037701	100.00	1.01	100.00	7.92	50.25	NM	P	N
21.	ANA4329694	100.00	2.20	87.77	31.36	56.11	NM	N	N
22.	ANA4501308	100.00	1.53	100.00	32.18	49.58	NM	P	N
23.	ANA4550544	100.00	0.93	100.00	14.79	50.29	NM	P	N
24.	ANA4604071	100.00	1.01	93.94	51.58	57.06	NM	N	N
25.	ANA4617085	100.00	1.01	93.94	51.58	57.06	NM	N	N
26.	ANA4741385	100.00	1.25	100.00	32.16	56.27	NM	P	N
27.	ANA4835276	100.00	0.30	99.63	7.10	54.59		N	N
28.	ANA5085235	94.33	7.40	91.76	23.06	35.29	NM	N	N
29.	ANA5201204	98.65	2.50	90.10	38.50	53.86	NM	P	N
30.	ANA5259689	100.00	0.98	99.83	29.92	49.58	NM	P	N
31.	ANA5588223	100.00	1.10	100.00	30.82	55.90	NM	N	N
32.	ANA5634920	94.49	0.73	99.53	54.77	20.53	NM	N	P
33.	ANA5635542	100.00	0.24	98.85	11.79	55.39	NM	P	P
34.	ANA5923031	96.51	0.74	81.69	255.06	0.54	NM	P	N
35.	ANA6055150	98.06	0.024	90.36	50.54	53.02	NM	P	N
36.	ANA6115436	96.26	0.37	96.49	12.62	39.24	NM	N	P
37.	ANA6263440	100.00	0.59	97.26	0.29	41.37	NM	P	N
38.	ANA6451816	100.00	0.45	94.09	36.53	56.91	NM	N	N
39.	ANA6917483	97.60	0.03	92.59	25.01	53.78	NM	N	P
40.	ANA6973880	100.00	0.97	95.47	26.74	47.71	NM	P	N
41.	ANA7055846	100.00	1.29	98.85	26.82	56.51	NM	P	N
42.	ANA7113102	100.00	1.29	98.85	26.82	56.51	NM	P	N
43.	ANA7145504	100.00	96.77	20.85	54.14	54.14	NM	P	P
44.	ANA7192589	98.80	0.08	93.07	23.28	55.64	NM	N	P

45.	ANA7296445	100.00	1.39	96.60	41.37	56.37	NM	P	N
46.	ANA7325519	100.00	2.28	98.54	12.19	52.39	NM	P	P
47.	ANA7438000	98.64	0.04	88.42	61.40	48.87	NM	N	N
48.	ANA7481255	97.64	0.04	93.86	3.23	52.75	NM	N	P
49.	ANA7527053	98.80	0.09	93.74	18.21	54.70	NM	P	P
50.	ANA7923580	100.00	1.66	94.99	0.05	42.14	NM	P	N
51.	ANA7963753	100.00	0.54	99.95	5.62	49.03	NM	P	P
52.	ANA7993024	97.94	2.12	89.90	349.33	22.07	NM	P	P
53.	ANA8430692	100.00	1.71	93.84	54.67	57.06	NM	N	N
54.	ANA8871618	97.40	3.08	91.94	36.53	33.60	NM	P	N
55.	ANA8886081	97.74	2.22	87.86	256.74	10.51	NM	N	P
56.	ANA8969446	97.83	0.02	90.54	327.49	31.75	NM	P	N

[#]HIA: Human intestinal absorption (Activity range: Poorly- 0~20%, Moderate- 20~70%, High- 70~100%)
[$]BBB: Blood brain barrier (CNS active compounds (+): >1, CNS inactive compounds (-): <1)
[@]PPB: Plasma protein Binding (Chemicals strongly bound > 90%, Chemicals weakly bound < 90%)
[&]MDCK: Madin-Darby canine kidney cell permeability (Lower- < 25, Moderate- 25~500, Higher- > 500)
[*]Caco2: Heterogeneous human epithelial colorectal adenocarcinoma cell permeability (Lower- <4, Moderate- 4~70, Higher- >70)
NM: Non-mutagen, M: Mutagen, P: Positive, N: Negative

3.3.3 Molecular docking of designed analogues

Among all analogues docked, ANA6917483 (ΔG: -10.44 kcal/mol) and ANA3550825 (ΔG: -10.31 kcal/mol) was found to bind strongly with the CYP1A1 followed by ANA3181590 (-10.27 kcal/mol), ANA7145504 (-10.24 kcal/mol), ANA4037701(-10.16 kcal/mol), ANA4550544 (-10.11 kcal/mol), ANA7192589 (-9.99 kcal/mol), ANA1222005 (-9.96 kcal/mol), ANA5259689 (-9.93 kcal/mol), and ANA4835276 (-9.89 kcal/mol). These ten hits exhibit better interactions with the target protein than ANF (-09.13 kcal/mol) and DBPD (-07.12 kcal/mol). The molecular interactions of CYP1A1with, the top 10 lead molecules and their comparison with the ANF and DBPD are shown in Table 3.3. Moreover, Cys422(H), Phe346, Ala428, His353(H), Arg71(H), Ile423, Trp96(H), Arg100(H), Arg420(H), Ser87, Ala282, Ile163, Gly424, Thr350, Ile351, Lue279, Thr286,

Ile414, Gly283, Phe415, Val347, Met86, Gly416, and Gln376 residues of CYP1A1 are engaged in molecular interactions with ANA6917483 (Figure 3.2). Likewise, Arg71(H), Trp96(H), Ile351, Arg100(H), Ser87, Arg420(H), Cys422(H), Ile423, Gly424, Ile163, Gly283, Ala282, Leu279, Thr286, Ala428, Phe415, Phe346, Ile414, Val347, Thr350, His353(H), Gly416, and Met86 residues of CYP1A1 are taking part in molecular interactions with the second-best analogue ANA3550825 (Figure 3.3).

Table 3.3. Molecular interactions of top 10 analogues, ANF, and DBPD with CYP1A1.

S. No.	Ligands	ADT (ΔG)	H-bonds
01.	ANA6917483	-10.44	TRP96-HE1…O, ARG100-HH11…O, ARG420-HH11…O, HEM601-ND…O, HEM601-ND…O, O…HEM601-O1D, O…HEM601-O2D
02.	ANA3550825	-10.31	ARG71-HH22…O, ARG100-HH11…O, ARG420-HH11…O, HEM601-HC…O, O…HEM601-O1D
03.	ANA3181590	-10.27	ARG71-HH22…F, ARG420-HH11…O, HEM601-ND…O
04.	ANA7145504	-10.24	ARG420-HH11…O, HEM601-ND…O
05.	ANA4037701	-10.16	ARG71-HH22…O, TRP96-HE1…F, ARG100-HH11…F, ARG420-HH11…F, HEM601-ND…O
06.	ANA4550544	-10.11	ARG420-HH11…O, HEM601-ND…O
07.	ANA7192589	-9.99	ARG71-HH22…O, HEM601-ND…O
08.	ANA1222005	-9.96	ARG71-HH22…O, HEM601-ND…O
09.	ANA5259689	-9.93	SER87-HG…O
10.	ANA4835276	-9.89	ARG420-HH11…O
11.	ANF	-09.13	O2…SER409-H, O2…VAL412-H
12.	DBPD	-07.12	V453-NH…O2

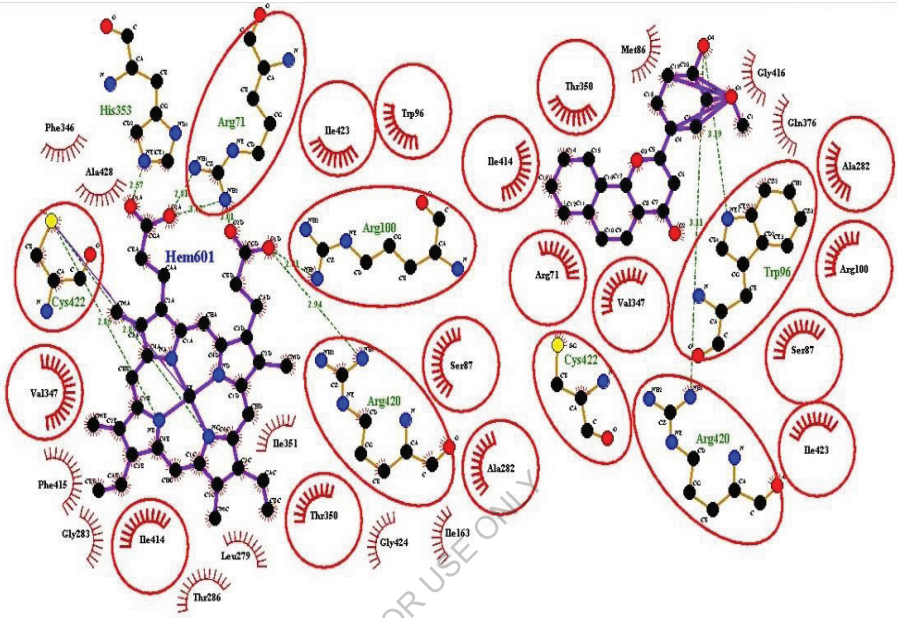

Figure 3.2. The 2D Ligplot of CYP1A1 with ANA6917483. Dashed lines (green) and arcs, respectively, represent H-bonds and hydrophobic contacts. Encircled residues are common in interaction with heme group and analogue.

Similarly, among all analogues docked, ANA8430692 (ΔG: -10.55 kcal/mol) and ANA7923580 (ΔG: -10.47 kcal/mol) was found to bind strongly with the CYP1A2 followed by ANA6451816 (-10.31 kcal/mol), ANA4637969 (-10.27 kcal/mol), ANA3421779 (-10.25 kcal/mol), ANA4329694 (-10.23 kcal/mol), ANA5085235 (-10.22 kcal/mol), ANA6055150 (-10.17 kcal/mol), ANA4604071 (-10.15 kcal/mol), and ANA2222312 (-10.11 kcal/mol). These ten hits depict better interactions with the target protein than ANF (-09.93 kcal/mol) and DBPD (-09.66 kcal/mol). The molecular interactions of CYP1A2 with the top ten lead molecules and their comparison with the ANF and DBPD are shown in Table 3.4. Moreover, Arg104(H), Ala284, Trp100(H),

Arg423(H), Arg75(H), Ile353, Thr91, His355(H), Thr352, Gly419, Cys425(H), Gln378, Leu90, Ala431, Leu349, Leu417, Thr288, Val289, Phe348(A), Phe343, Ile435, Phe438, Gly285, Gly427, Leu111, Ile426, and Ile281 residues of CYP1A2 are engaged in molecular interactions with ANA8430692 (Figure 3.4). Similarly, Trp100(H), Arg423(H), Arg75(H), Thr91, His355(H), Ile353, Asp280, Leu90, Phe418, Ala284, Gly419, Thr352, Ile426, Leu417(A), Gln378, Thr288, Phe348, Leu349, Phe343, Ile435, Val289, Cys425(H), Ile281, Gly427, Ala431, Leu111, Arg104(H), and Gly285 residues of CYP1A2 are playing major roles in molecular interactions with the second-best analogue ANA7923580 (Figure 3.5).

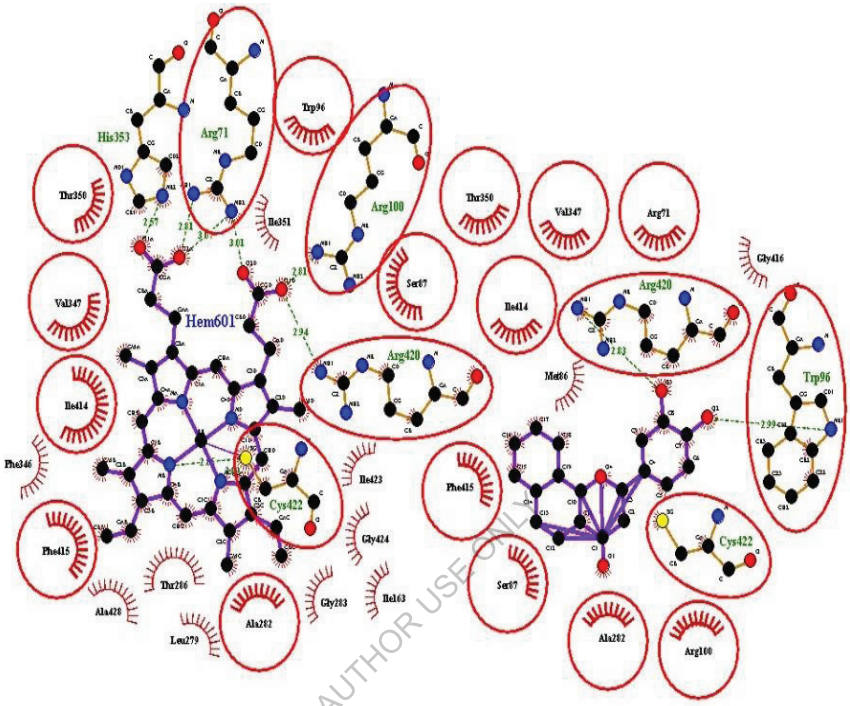

Figure 3.3. The 2D Ligplot of CYP1A1 with ANA3550825. Dashed lines (green) and arcs, respectively, represent H-bonds and hydrophobic contacts. Encircled residues are common in interaction with heme group and analogue.

Table 3.4. Molecular interactions of top 10 analogues, ANF, and DBPD with CYP1A2.

S. No.	Ligands	ADT (ΔG)	H-bonds
01.	ANA8430692	-10.55	ARG75-HH11…O, ARG75-HH21…O, HIS355-HE2…O, HEM900-HA…O, HEM900-HB…O, HEM900-HD…O, O…HEM900-O1A, O…HEM900:O2A
02.	ANA7923580	-10.47	ARG75-HH21…O, ARG423-HH11…O

03.	ANA6451816	-10.31	ARG75-HH22…O
04.	ANA4637969	-10.27	ARG75-HH21…F
05.	ANA3421779	-10.25	TRP100-HE1…Cl, ARG423-HH11…Cl
06.	ANA4329694	-10.23	ASN214-HN…O6
07.	ANA5085235	-10.22	ARG75-HH22…O
08.	ANA6055150	-10.17	ARG75-HH22…O
09.	ANA4604071	-10.15	ARG75-HH22…O
10.	ANA2222312	-10.11	ILE353-HN…O
11.	ANF	-09.93	ARG263-HN…O1
12.	DBPD	-09.66	H42…ALA102-O

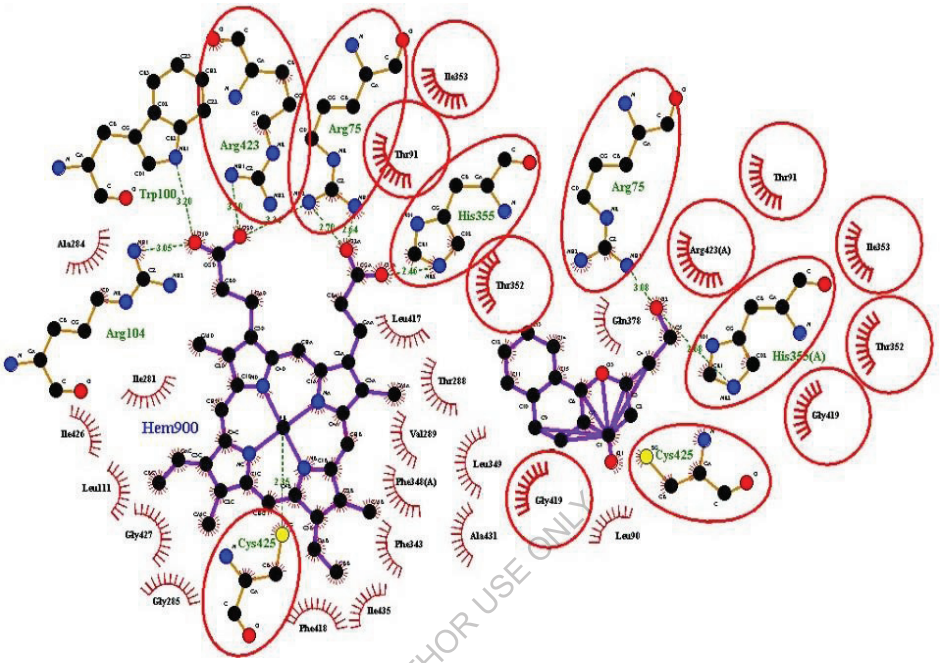

Figure 3.4. The 2D Ligplot of CYP1A2 with ANA8430692. Dashed lines (green) and arcs, respectively, represent H-bonds and hydrophobic contacts. Encircled residues are common in interaction with heme group and analogue.

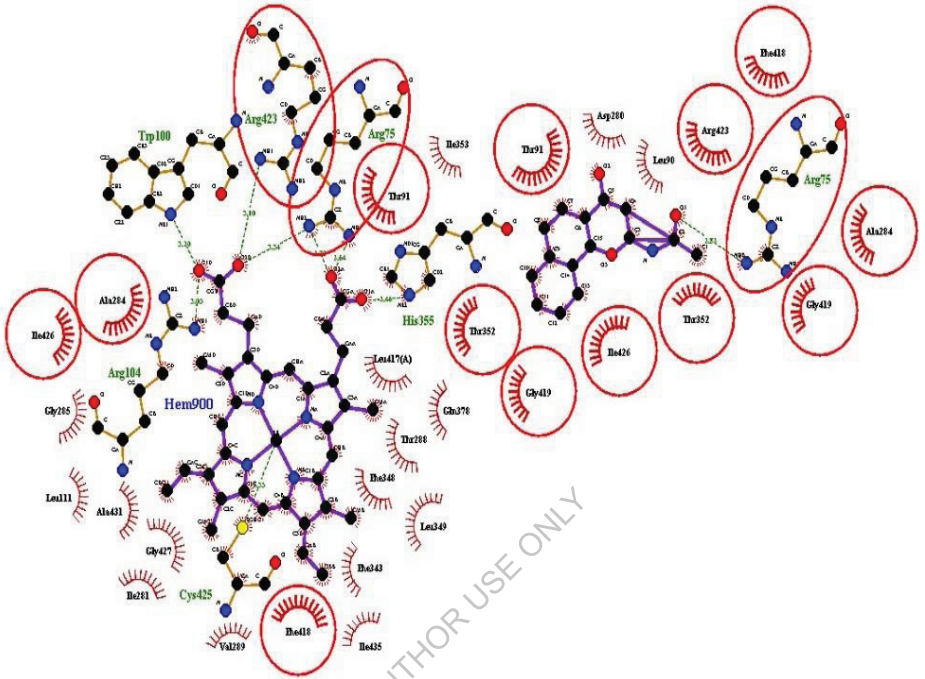

Figure 3.5. The 2D Ligplot of CYP1A2 with ANA7923580. Dashed lines (green) and arcs, respectively, represent H-bonds and hydrophobic contacts. Encircled residues are common in interaction with heme group and analogue.

Likewise, among all analogues docked, ANA6451816 (ΔG: -10.14 kcal/mol) and ANA4501308 (ΔG: -10.02 kcal/mol) was found to bind strongly with the CYP1B1 followed by ANA3550825 (-10.01 kcal/mol), ANA3181590 (-09.90 kcal/mol), ANA3484613 (-09.88 kcal/mol), ANA2685819 (-09.85 kcal/mol), ANA4550544 (-09.75 kcal/mol), ANA2113872 (-09.69 kcal/mol), ANA4604071 (-09.64 kcal/mol), and ANA4329694 (-09.44 kcal/mol). ANF (-09.93 kcal/mol) and DBPD (-09.66 kcal/mol) exhibit better binding with CYP1B1 as compared to CYP1A1 and 1A2. The molecular interactions of CYP1B1 with the top ten lead molecules and their comparison with the

ANF and DBPD are shown in Table 3.5. Moreover, Ser393(H), His330(H), Thr327, Ile328, Arg50(H), Trp74, Arg397(H), Ala66, Met65, Arg78(H), Ile400, Cys399(H), Gly401, Met85, Ser260, Ile256, Ala259, Ile391, Thr263, Phe392, Leu264, Ser405, Leu409, Val324, Phe323, and Gln353 residues of CYP1B1 are engaged in molecular interactions with ANA6451816 (Figure 3.6). Similarly, His330(H), Ser393(H), Thr327, Ile328, Arg50(H), Ala66, Arg397(A)(H), Met65, Arg78(H), Trp74, Ile400, Met85, Gly401, Ile256, Ala259, Cys399(H), Gln353(H), Ser405, Ser260, Leu264, Leu409, Thr263, Ile391, Phe323, Val324, Phe392 residues of CYP1B1 are key players in molecular interactions with the second-best analogue ANA (Figure 3.7).

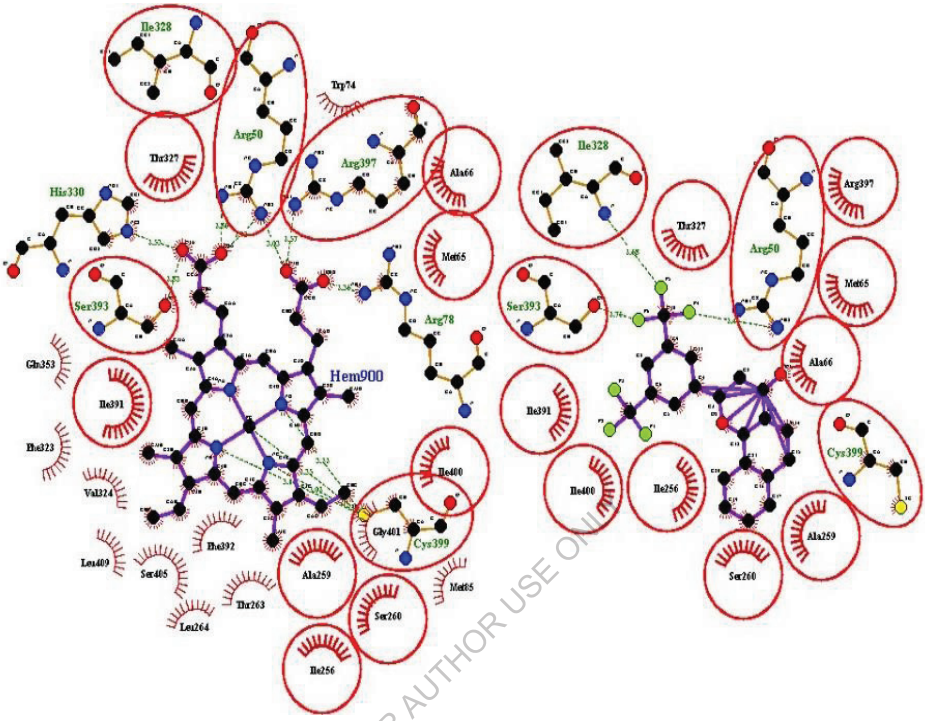

Figure 3.6. The 2D Ligplot of CYP1B1 with ANA6451816. Dashed lines (green) and arcs, respectively, represent H-bonds and hydrophobic contacts. Encircled residues are common in interaction with heme group and analogue.

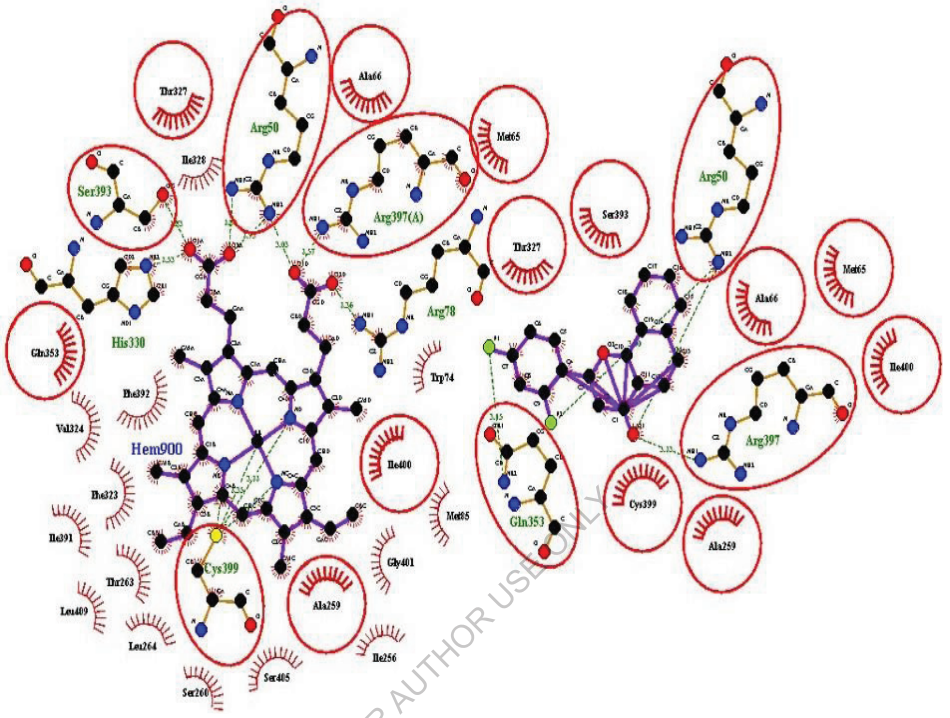

Figure 3.7. The 2D Ligplot of CYP1B1 with ANA4501308 Dashed lines (green) and arcs, respectively, represent H-bonds and hydrophobic contacts. Encircled residues are common in interaction with heme group and analogue.

Table 3.5. Molecular interactions of top 10 analogues, ANF, and DBPD with CYP1B1.

S. No.	Ligands	ADT (ΔG)	H-bonds
01.	ANA6451816	-10.14	ARG50-HH22…F, ILE328-HN…F, SER393-HG…F, HEM900-HA…F, HEM900-HB…F, HEM900-HD…O
02.	ANA4501308	-10.02	TRP96-HE1…O, ARG50-HH21…O, ARG50-HH22…F, ARG397-HH12…O
03.	ANA3550825	-10.01	LEU404-HN…O9
04.	ANA3181590	-9.90	ARG50-HH21…O, HEM900-HD…O
05.	ANA3484613	-9.88	ARG50-HH22…O, HEM900-HA…O
06.	ANA2685819	-9.85	ARG50-HH21…O, HEM900-HA…F, HEM900-HB…F
07.	ANA4550544	-9.75	ARG50-HH21…O, HEM900-HA…Cl, HEM900-HB…Cl, HEM900-HD…Cl, HEM900-HD…O
08.	ANA2113872	-9.69	ARG50-HH22…O, HEM900-HA…O, HEM900-HD…O
09.	ANA4604071	-9.64	LYS443-HZ1…O9
10.	ANA4329694	-9.44	ARG50-HH21…O, HEM900-HD..O
11.	ANF	-09.67	ARG373-HH12…O2
12.	DBPD	-10.08	TRP354-HE1…O2

3.3.4 MD Simulation

The explicit solvent MD simulation of CYP1A2 with the designed compound and the known inhibitors shows considerable stability at the simulation point. Overall simulation of the complexes was carried for 30ns, and the protein remained stable. The docked poses of the four complexes were utilized for the simulation studies. The stability of the protein-ligand complex of protein CYP1A2 with four compounds was analyzed. RMSD graph of protein CYP1A2 with the ligand complex reveals that the overall RMSD is around 1-3.5 Å. Figure 3.8 represents the RMSD, and Figure 3.9 represents the RMSF graph of the complexes. RMSD graph indicates the stability and looking in profound to the Root mean square deviation (RMSD), the blue color represents the designed ligand ANA8430692, red and black represents the ANF, and DBPD gray represents second ligand ANA7923580. The overall graph states that the RMSD of the protein with the ligand ANA8430692 shows more stability when compared to other complexes. The stability of the compound is due to the interaction between the protein and the ligand. The RMSF graph states that there are no significant fluctuations for the compounds, and with the region from the residue 180 to 200, the residues fluctuated. This fluctuation is observed throughout all the compounds. Figure 3.10 represents the radius of gyration, which states that the compactness of the protein is maintained throughout the analysis. On the overall study, it was concluded that the complexes show considerable stability throughout the simulation. MD studies reveal that the compounds ANA8430692 are comparatively stable during the entire process of 30 ns simulation.

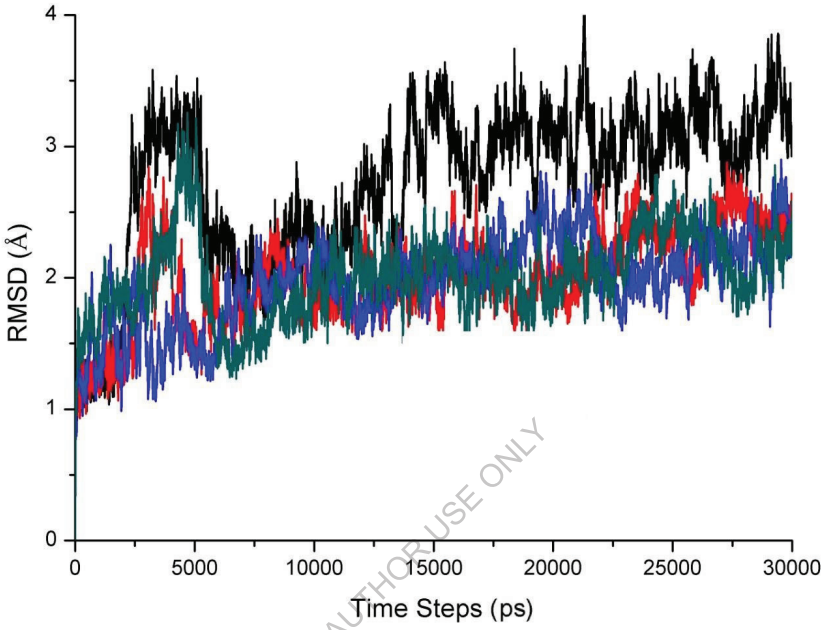

Figure 3.8. MD simulation of ligands binding to the CYP1A2. RMSD plot as a function of time. Black, red, blue, and grey colors represent DBPD, ANF, ANA8430692, and ANA7923580 respectively.

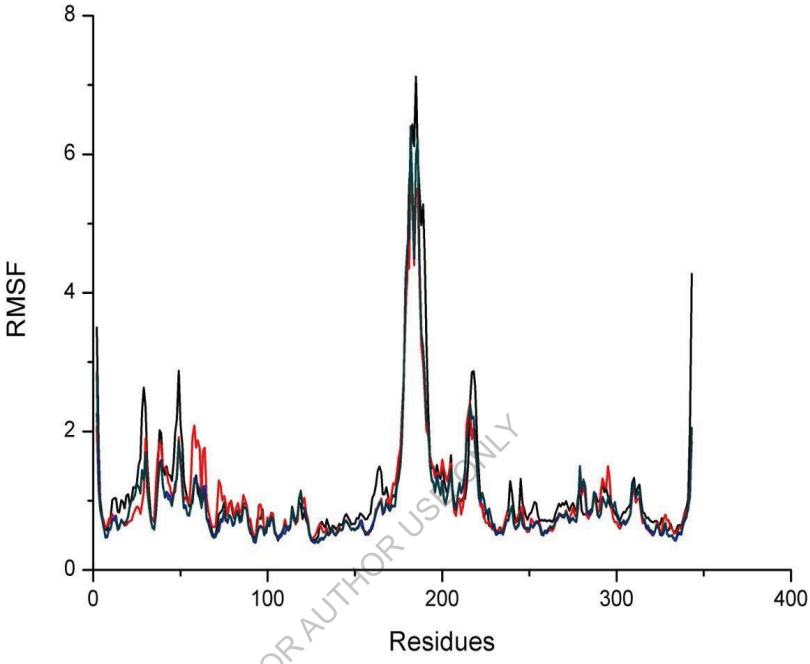

Figure 3.9. MD simulation of ligands binding to the CYP1A2. RMSF plot for DBPD (black), ANF (red), ANA8430692 (blue), and ANA7923580 (grey).

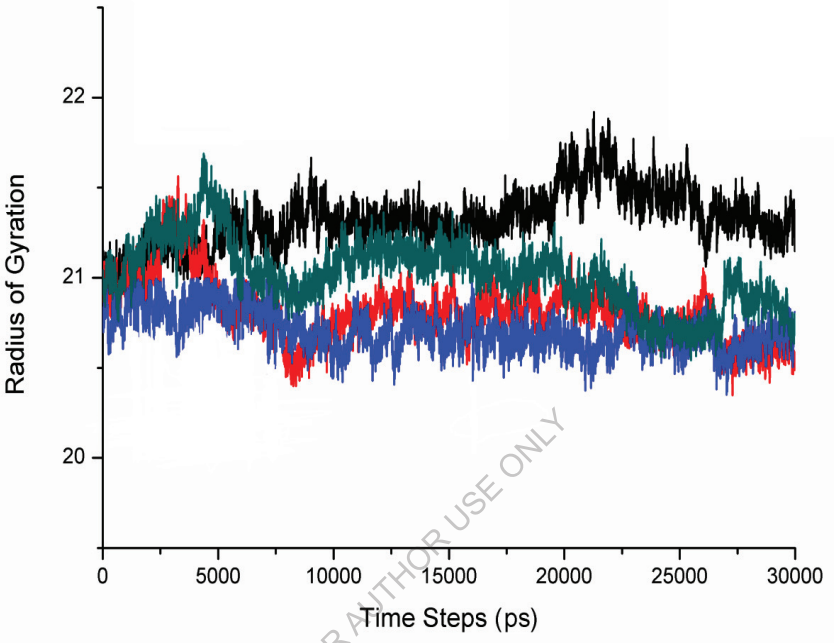

Figure 3.10. MD simulation of ligands binding to the CYP1A2. Time evolution of Rg values of DBPD (black), ANF (red), ANA8430692 (blue) and ANA7923580 (grey) during 30 ns MD simulation.

3.4 Conclusion

In this work, combinatorial design, computational ADMET, molecular docking, and MD studies were carried to identify potent inhibitors for CYP1A1, 1A2, and 1B1. Initially, ANF was taken as a template for screening and docked into the active site of CYP450 isozymes for binding mode analysis. Analogues showing best interactions with target protein was carried out for MD simulation of 30 ns duration. The proposed best docked binding poses were essentially maintained during the whole process of MD simulation.

The same H-bonding interactions and occupancy have been shown during 30 ns simulations. The MD simulation results provide an appropriate start point for further screening of chemical drug-likeness combinatorial library design substrate analogue. Non-toxic molecules (carcinogenicity, mutagenicity rat models) were filtered from 400 screened hits. Lipinski RO5 has yielded 88 molecules following its 3 out of 4 rules. The ADME filters were also applied for non-toxic filtered molecules using solubility, absorption, polar surface area, and blood-brain barrier criteria. This effort leads to 56 hits from the combinatorial library. Molecular docking studies were carried out using AutoDock4.0 tools. Best docked conformation was selected using criteria; H-bonding interaction with active site residues, binding energy, and best fit into the active site of target proteins. Finally, the top ten hits against each isozyme were compared with DBPD and ANF. These hits were showing stronger binding with their respective isozymes as compared to the carcinogen and known inhibitor. Moreover, MD studies of the top two lead molecules of CYP 1A2, ANF, and DBPD were carried out for 30ns duration that favors the stability of ANA8430692 followed by ANA7923580. These analogues might be used as a potent inhibitor against CYP1A2.

Chapter-4 *In vitro* validation and elucidation of putative lead candidate(s)

4.1 Introduction

Cancer development is usually a multistep mechanism driven by genetic and epigenetic damage caused by carcinogens in susceptible cells resulting in a selective growth advantage. Consequently, clonal expansion of the cells may occur due to proto-oncogene activation and tumor suppressor genes inactivation. About 100 different cancers are present, and subtypes of cancers can be located within specific tissues, resulting in almost limitless combinations of genetic and epigenetic changes. Different mature cells in the body have given a life period. After a fixed life span, these cells die, new cells are generated by the proliferation and differentiation of various stem cells. Under normal circumstances, the production of the new cell remains constant. Occasionally though, cells arise that no longer respond to the normal growth-control mechanism. Uncontrolled growth of cells results in neoplastic cells. Tumors are classified as benign or malignant, and their study is called oncology. Benign cells are enclosed in a capsule, whereas malignant tumors are not encapsulated and invasive thereby, cancer cells undergo angiogenesis and metastasis. Malignancy is present when metastasis establishes a new tumor distant from the primary tumor.

The overall process of converting the normal cells to malignant cells is named as carcinogenesis, which might be set off by etiologic factors, cancer-causing chemical substances, radiation, irresistible organic matters, or endogenous factors, viz., acquired changes, up-regulation of chemicals, and abnormality in body's immunities. CYP450 isoenzymes are heme-containing proteins that go about as oxidoreductases. CYP1 sub-group of proteins are associated with the metabolism of enormous xenobiotics viz.

(PAHs, mutagens, adulterants, and estrogens to cytotoxic, mutagenic, and cancer-causing chemicals.[55-157] Within sight of PAH ligands, AhR move to the nucleus where it binds with the other inducer proteins of CYP450s which prompts the enlistment and over-articulation of CYP450s proteins. These overexpressed chemicals, this way, utilize PAHs into cancer-causing intermediates, which eventually harm DNA. The AhR-interceded mechanism actuated in cells against PAHs gives a chance to use CYP450s as therapeutic targets to forestall carcinogenesis in such cells.[158-160]

Breast carcinoma is the most frequently reported aggressive malignancy and the second major cause of death among females after lung cancer globally. It is more likely to occur as women get older, but it can occur in younger women too. From the last few decades, it has been well established that CYP450 isozymes are promising therapeutic targets in various environmental carcinogen-induced cancers. Identifying and designing new chemical entities that restrain CYP450s is explicitly a space of extraordinary interest. These inhibitors could assume a significant part in chemotherapeutic prevention and cure. CYP450s are essential for the human body's stage I metabolic framework and get initiated uniquely in those tissues that manage cancer-causing agents' metabolism.

In the absentia of cancer-inducing agents, the cellular concentration CYP1A1 is fundamentally low and does not meddle with the typical metabolic cycle of the human body. CYP1A1 isozyme being practically comparative, they vary from CYP1A2 and CYP1B1 in the underlying model of actions depending on the nature of substrate molecules, although CYP1A1 and CYP1A2 are about 72% homologous in their sequences and CYP1B1 exhibits about 38% homology. This chapter is based on our *in vitro* work, which targets CYP 1A1, 1A2, and 1B1 in the MCF7 breast cancer cell line.

The best lead obtained after post docking analysis, MD simulation, and comparison with known inhibitor ANF succeeded through (3-(4, 5-dimethylthiazolyl-2)-2,5-diphenyltetrazolium bromide) (MTT) and enzyme inhibition assays elucidating potential putative lead molecules against respective CYP450 isozymes.

4.2 Materials and methods

4.2.1 Chemicals and reagents

Chemical compounds CHEMBL1 (6-iodo-4'-methoxyflavone), CHEMBL2 (3',4'-dimethoxy-alpha-naphthoflavone), and CHEMBL3 (6-fluoroflavone) from Sigma-Aldrich St. Louis, MO. MCF-7 cell line from NCCS Pune India, PBS, penicillin, streptomycin, and MTT dye from HiMedia Laboratories India, ANF (7,8-benzoflavone), EMEM, FBS, and DMSO was procured from Sigma-Aldrich St. Louis, MO.

4.2.2 Cell culture

The MCF-7 cells were maintained in EMEM supplemented with 10% FBS, 0.01 mg/ml insulin, and 1% penicillin/streptomycin.

4.2.3 MTT cell viability assay

Using the MTT dye, colorimetric cell viability assays were conducted according to the manufacturer's protocol [29]. The mitochondrial dehydrogenases in viable cells reduced the tetrazolium ring of MTT, converting the yellow-coloured MTT to purple formazan crystals. For each well, 5000 cells per were seeded in a 96-well plate, allowed to attach overnight, and then treated with ANF (0-100 μM) or CHEMBL1, CHEMBL2, and CHEMBL3 (0-100 μM) for 24 h. Cell viability was quantified at 540 nm using the BioTek plate reader (BioTek, Winooski, VT). Data were normalized to the vehicle control, DMSO, and collected from three independent experiments.

4.2.4 *In vitro* CYP450 enzyme assay

For *in vitro* CYP450 enzyme assay, MCF-7 (1 x 106) were seeded in triplicates in black 96-well plates with transparent bottom. The test compounds at various concentrations (from 1-1000 nM) were added to the wells, followed by incubation at 37°C, 5% CO2 for 30 min. After incubation, a fluorogenic substrate 7-ER (7-Ethoxyresorufin) for CYP1A1, CYP1B1, and CEC (3-cyano-7-ethoxycoumarin) for CYP1A2 was added at five μM concentration to the wells, and contents mixed by shaking. The plate was read on a plate reader (Biotek, Synergy HT) for 60 min using suitable wavelengths for emission/excitation of the fluorescence products formed. Data were normalized to vehicle control, DMSO and collected from three independent experiments.

4.2.5 Statistical analysis

Statistical analyses of the experimental data were performed using GraphPad Prism8, GraphPad Software, Inc., La Jolla, CA, USA. Either the two-sided t-test or one-way analysis of variance (ANOVA) was performed. The value $p<0.01$ was considered significant.

4.3 Results and discussion

4.3.1 MTT assay

The lead compounds CHEMBL1, 2, and 3 identified via in silico strategies were tested for their in vitro antiproliferative activity against the human breast cancer cell line MCF-7 at different concentrations (0-100 μM) by MTT assay. The cell inhibition percentages of tested compounds were determined after measuring at 24 hours of exposure. The CHEMBL1 showed a 50% cytotoxic effect on the MCF-7 cell line at 29.69 μM, and

CHEMBL2 showed the cytotoxic effect at 13.56 μM, whereas CHEMBL3 showed 50% cytotoxic effect on MCF-7 cell line at 8.36 μM (Figure 4.1, 4.2 and 4.3). As shown in Figure 4.1 to 4.3, compounds 1, 2, and 3 were found to inhibit the growth of breast cancer cell line MCF-7 potently, and its activity was significantly different from ANF at 25, 50, and 100 μM doses.[161-164] Moreover, the MTT assay results suggested that CHEMBL3 was found to be the most potent against the MCF-7 cell line (Figure 4.3) and could be probed further to delineate its strong anti-cancer potential.

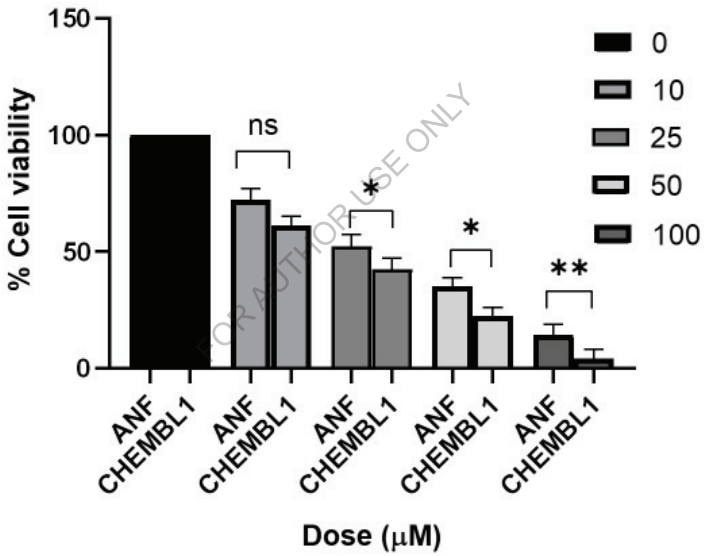

Figure 4.1. Dose dependent inhibition of cell viability of breast cancer cell line MCF-7 by alpha-naphthoflavone (ANF) and CHEMBL1. The data is Mean±SD of three independent experiments repeated thrice (*p<0.01, **p<0.001 were considered significant; ns represents non-significant).

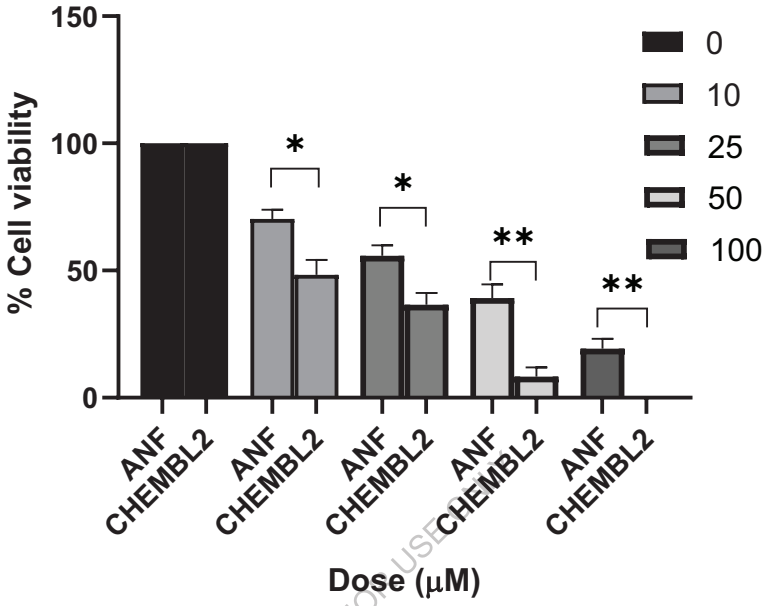

Figure 4.2. Dose dependent inhibition of cell viability of breast cancer cell line MCF-7 by alpha-naphthoflavone (ANF) and CHEMBL2. The data is Mean±SD of three independent experiments repeated thrice (*p<0.01, **p<0.001 were considered significant; ns represents non-significant).

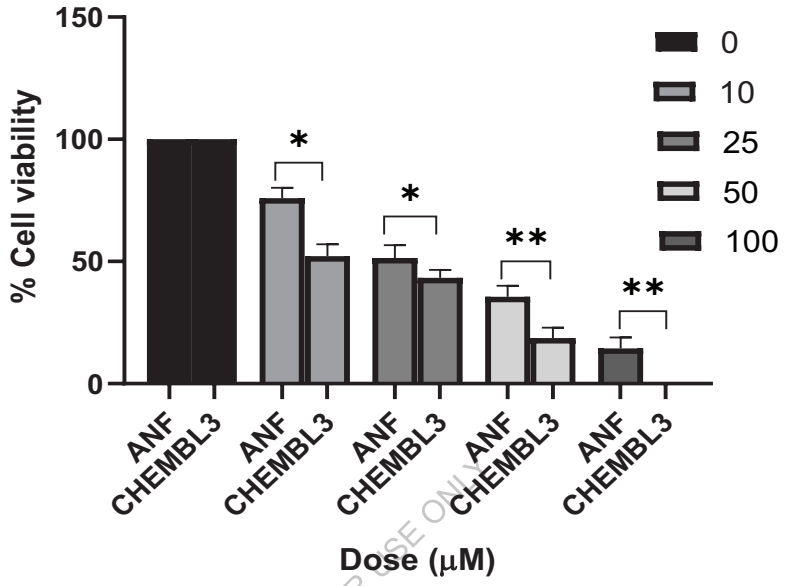

Figure 4.3. Dose dependent inhibition of cell viability of breast cancer cell line MCF-7 by alpha-naphthoflavone (ANF) and CHEMBL3. The data is Mean±SD of three independent experiments repeated thrice (*p<0.01, **p<0.001 were considered significant; ns represents non-significant).

4.3.2 Enzyme inhibition assay

The inhibition of various CYP enzymes activity by CHEMBL1, 2, and 3 were measured using a specific substrate described in Materials and Methods. Our results have shown that CHEMBL1, 2, and 3 inhibited CYP1A1, CYP1A2, and CYP1B1 enzyme activity in a dose-dependent manner.[165,166] CHEMBL1 (50-1000 nM) significantly inhibited CYP1A1 activity, and the inhibition was significantly different from ANF, a known CYP1A1 inhibitor, at 100, 200, and 500 nM dose. Similarly, CHEMBL2 (50-1000 nM) showed potent inhibition of CYP1A2 activity, and the reduction in the activity was

significantly different from ANF at 100, 200, and 500nM doses. Moreover, CHEMBL3 (50-1000 nM) potently inhibited the CYP1B1 activity, and the inhibition was significantly different from ANF at 100, 200, and 500 nM doses. Therefore, our results suggest that inhibition of CYP1A1, CYP1A2, and CYP1B1 enzymes by our proposed compounds could prevent DBP-induced mammary cancer because of suppression of carcinogenic activation of DBP (Figure 4.4, 4.5 and 4,6).

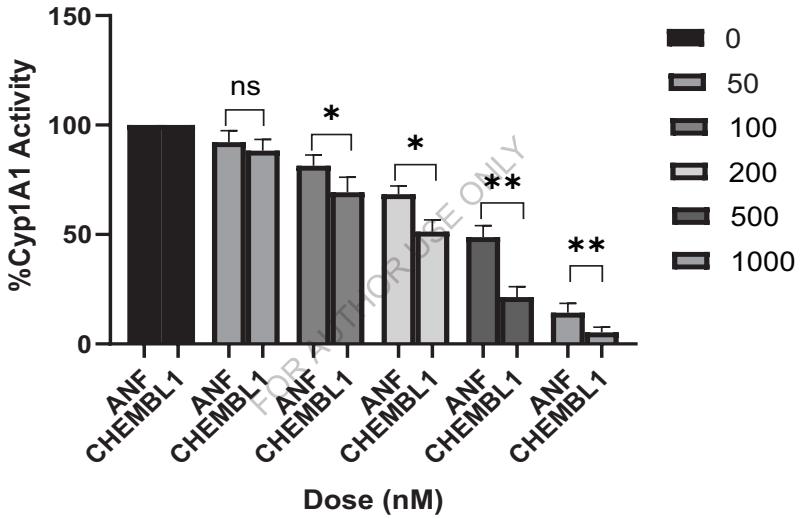

Figure 4.4. Inhibition of CYP1A1 enzyme activity in breast cancer cell line MCF-7 by alpha-naphthoflavone (ANF) and CHEMBL1. The data is Mean±SD of three independent experiments repeated thrice (*p<0.01, **p<0.001 were considered significant; ns represents non-significant).

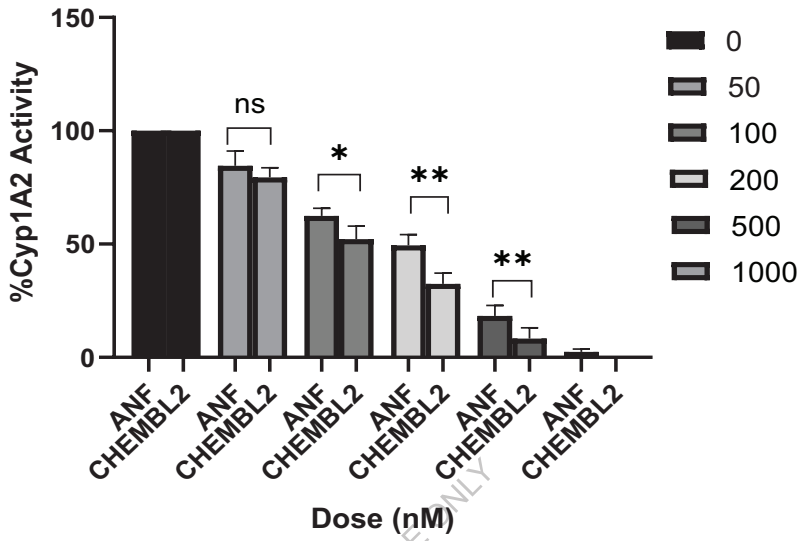

Figure 4.5. Inhibition of CYP1A2 enzyme activity in breast cancer cell line MCF-7 by alpha-naphthoflavone (ANF) and CHEMBL2. The data is Mean±SD of three independent experiments repeated thrice (*p<0.01, **p<0.001 were considered significant; ns represents non-significant).

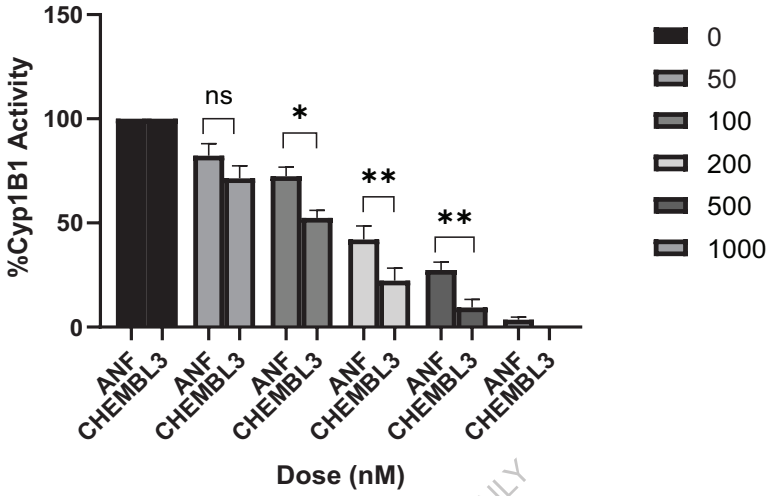

Figure 4.6. Inhibition of CYP1B1 enzyme activity in breast cancer cell line MCF-7 by alpha-naphthoflavone (ANF) and CHEMBL3. The data is Mean±SD of three independent experiments repeated thrice (*p<0.01, **p<0.001 were considered significant; ns represents non-significant).

4.4 Conclusion

Lead compounds, namely CHEMBL1, 2, and 3 identified through RO5, and ADMET filtration, molecular docking, and MD simulation process, were tested for *in vitro* antiproliferative activity against the human breast cancer cell line MCF-7 at different concentrations (0-100 μM) by MTT assay. The findings of the MTT assay exhibits that CHEMBL3 is showed greater efficacy against the MCF-7 cell line. Likewise, an inhibition assay was also performed for aforesaid putative lead molecules. The findings suggest that CHEMBL3 (50-1000 nM) efficiently inhibited the CYP1B1 activity, and it was significantly different from ANF at 100, 200, and 500 nM doses. Therefore, our results suggest that inhibition of CYP1A1, CYP1A2, and CYP1B1

enzymes by our proposed compounds could prevent DBP-induced mammary cancer because of suppression of carcinogenic activation of DBP and might be open a new door for designing new drug candidates against PAH-induced breast cancer.

BIBLIOGRAPHY

1. DeSantis CE, Bray F, Ferlay J, Lortet-Tieulent J, Anderson BO, Jemal A. International Variation in Female Breast Cancer Incidence and Mortality Rates. Cancer Epidemiol Biomarkers Prev. 2015;24(10):1495–506.
2. Ginsburg O, Yip C, Brooks A, Cabanes A, Caleffi M, Dunstan Yataco JA, et al. Breast cancer early detection: A phased approach to implementation. Cancer. 2020;126(S10):2379–93.
3. Velazquez Berumen A, Jimenez Moyao G, Rodriguez NM, Ilbawi AM, Migliore A, Shulman LN. Defining priority medical devices for cancer management: a WHO initiative. Lancet Oncol. 2018;19(12):e709–19.
4. Ilbawi AM, Velazquez-Berumen A. World Health Organization List of Priority Medical Devices for Cancer Management to Promote Universal Coverage. Clin Lab Med. 2018;38(1):151–60.
5. Rositch AF, Unger-Saldaña K, DeBoer RJ, Ng'ang'a A, Weiner BJ. The role of dissemination and implementation science in global breast cancer control programs: Frameworks, methods, and examples. Cancer. 2020;126(S10):2394–404.
6. Wild CP, E W, Stewart BW. World cancer report: Cancer Research for Cancer Prevention. Lyon, France: International Agency for Research on Cancer. World Health Organization. 2020. 15-91.
7. Barrios CH, Reinert T, Werutsky G. Global Breast Cancer Research: Moving Forward. Am Soc Clin Oncol Educ B. 2018;(38):441–50.

8. Azamjah N, Soltan-Zadeh Y, Zayeri F. Global Trend of Breast Cancer Mortality Rate: A 25- Birkett N, Al-Zoughool M, Bird M, Baan RA, Zielinski J, Krewski D. Overview of biological mechanisms of human carcinogens. J Toxicol Environ Heal Part B. 2019;22(7–8):288–359.

9. Soerjomataram I, Bray F. Planning for tomorrow: global cancer incidence and the role of prevention 2020-2070. Nat Rev Clin Oncol 2021. Jun 2; 1-10

10. Birkett N, Al-Zoughool M, Bird M, Baan RA, Zielinski J, Krewski D. Overview of biological mechanisms of human carcinogens. J Toxicol Environ Heal Part B. 2019;22(7–8):288–359.

11. Barupal DK, Schubauer-Berigan MK, Korenjak M, Zavadil J, Guyton KZ. Prioritizing cancer hazard assessments for IARC Monographs using an integrated approach of database fusion and text mining. Environ Int. 2021;156:106624.

12. Rodu B, Cole P, Mandel JS. Evaluation of the National Toxicology Program Report on Carcinogens. Regul Toxicol Pharmacol. 2012. 64(1):186–8.

13. Goodman JE, Mayfield DB, Becker RA, Hartigan SB, Erraguntla NK. Recommendations for further revisions to improve the International Agency for Research on Cancer (IARC) Monograph program. Regul Toxicol Pharmacol. 2020;113:104639.

14. Suarez-Torres JD, Alzate JP, Orjuela-Ramirez ME. The NTP Report on Carcinogens: A valuable resource for public health, a challenge for regulatory science. J Appl Toxicol. 2020;40(1):169–75.

15. Identification of Potential Lead Molecules against Dibenzo[a,l]pyrene-induced Mammary Cancer through Targeting Cytochrome P450 1A1, 1A2, and 1B1 Isozymes. Biointerface Res Appl Chem. 2021;12(1):1096–109.

16. Arif J. Microsome-mediated bioactivation of dibenzo[a,l]pyrene and identification of DNA adducts by 32P-postlabeling. Carcinogenesis. 1997;18(10):1999–2007.

17. Khan MKA, Akhtar S, Arif JM. Development of In Silico Protocols to Predict Structural Insights into the Metabolic Activation Pathways of Xenobiotics. Interdiscip Sci Comput Life Sci. 2018;10(2):329–45.

18. Gupta RC, Arif JM, Gairola CG. Enhancement of pre-existing DNA adducts in rodents exposed to cigarette smoke. Mutat Res Mol Mech Mutagen. 1999;424(1–2):195–205.

19. Smith JN, Mehinagic D, Nag S, Crowell SR, Corley RA. In vitro metabolism of benzo[a]pyrene-7,8-dihydrodiol and dibenzo[def,p]chrysene-11,12 diol in rodent and human hepatic microsomes. Toxicol Lett. 2017;269:23–32.

20. Smith WA, Arif JM, Gupta RC. 1,2-dithiole-3-thione and its structural analogue oltipraz are potent inhibitors of dibenzo[a,l]pyrene-DNA adduction in female Sprague-Dawley rats. Int J Cancer. 2001;91(1):132–6.

21. Chen K-M, Guttenplan JB, Zhang S-M, Aliaga C, Cooper TK, Sun Y-W, et al. Mechanisms of oral carcinogenesis induced by dibenzo[a,l]pyrene: An environmental pollutant and a tobacco smoke constituent. Int J Cancer. 2013;133(6):1300–9.

22. Shou M, Krausz KW, Gonzalez FJ, Gelboin H V. Metabolic activation of the potent carcinogen dibenzo[a,l]pyrene by human recombinant cytochromes P450, lung and liver microsomes. Carcinogenesis. 1996;17(11):2429–33.

23. Siddens LK, Bunde KL, Harper TA, McQuistan TJ, Löhr C V., Bramer LM, et al. Cytochrome P450 1b1 in polycyclic aromatic hydrocarbon (PAH)-induced skin carcinogenesis: Tumorigenicity of individual PAHs and coal-tar extract, DNA adduction and expression of select genes in the Cyp1b1 knockout mouse. Toxicol Appl Pharmacol. 2015;287(2):149–60.

24. Siddens LK, Larkin A, Krueger SK, Bradfield CA, Waters KM, Tilton SC, et al. Polycyclic aromatic hydrocarbons as skin carcinogens: Comparison of benzo[a]pyrene, dibenzo[def,p]chrysene and three environmental mixtures in the FVB/N mouse. Toxicol Appl Pharmacol. 2012;264(3):377–86.

25. Manikandan P, Nagini S. Cytochrome P450 Structure, Function and Clinical Significance: A Review. Curr Drug Targets. 2018;19(1):38–54.

26. Munro AW, McLean KJ, Grant JL, Makris TM. Structure and function of the cytochrome P450 peroxygenase enzymes. Biochem Soc Trans. 2018;46(1):183–96.

27. Barnaba C, Gentry K, Sumangala N, Ramamoorthy A. The catalytic function of cytochrome P450 is entwined with its membrane-bound nature. F1000Research. 2017;6:662.

28. Rendic SP, Guengerich FP. Human Family 1–4 cytochrome P450 enzymes involved in the metabolic activation of xenobiotic and physiological chemicals: an update. Arch Toxicol. 2021;95(2):395–472.

29. Shimada T, Guengerich FP. Inhibition of Human Cytochrome P450 1A1-, 1A2-, and 1B1-Mediated Activation of Procarcinogens to Genotoxic Metabolites by Polycyclic Aromatic Hydrocarbons. Chem Res Toxicol. 2006;19(2):288–94.

30. Smith JN, Mehinagic D, Nag S, Crowell SR, Corley RA. In vitro metabolism of benzo[a]pyrene-7,8-dihydrodiol and dibenzo[def,p]chrysene-11,12 diol in rodent and human hepatic microsomes. Toxicol Lett. 2017;269:23–32.

31. Nakano N, Sakata N, Katsu Y, Nochise D, Sato E, Takahashi Y, et al. Dissociation of the AhR/ARNT complex by TGF-β/Smad signaling represses CYP1A1 gene expression and inhibits benze[a]pyrene-mediated cytotoxicity. J Biol Chem. 2020;295(27):9033–51.

32. Androutsopoulos VP, Tsatsakis AM, Spandidos DA. Cytochrome P450 CYP1A1: wider roles in cancer progression and prevention. BMC Cancer. 2009;9(1):187.

33. Sayer JM, Yagi H, van Bladeren PJ, Levin W, Jerina DM. Stereoselectivity of microsomal epoxide hydrolase toward diol epoxides and tetrahydroepoxides derived from benz[a]anthracene. J Biol Chem. 1985;260(3):1630–40.

34. Dock L, Waern F, Martinez M, Grover PL, Jernström B. Studies on the further activation of benzo[a]pyrene diol epoxides by rat liver microsomes and nuclei. Chem Biol Interact. 1986;58(C):301–18.

35. Jernström B, Mannervik B, Funk M, Seidel A. Glutathione Transferase A1-1 Catalyzed Conjugation of Polycyclic Aromatic Hydrocarbon Diol-Epoxides with Glutathione. Polycycl Aromat Compd. 1996;10(1–4):51–7.

36. Hengstler JG, Arand M, Herrero ME, Oesch F. Polymorphisms of N-Acetyltransferases, Glutathione S-Transferases, Microsomal Epoxide Hydrolase

and Sulfotransferases: Influence on Cancer Susceptibility. In: Recent results in cancer research Fortschritte der Krebsforschung Progrès dans les recherches sur le cancer. 1998. p. 47–85.

37. Mitrunen K, Jourenkova N, Kataja V, Eskelinen M, Kosma VM, Benhamou S, et al. Glutathione S-transferase M1, M3, P1, and T1 genetic polymorphisms and susceptibility to breast cancer. Cancer Epidemiol Biomarkers Prev. 2001;10(3):229–36.

38. Song Z, Shao C, Feng C, Lu Y, Gao Y, Dong C. Association of glutathione S-transferase T1, M1, and P1 polymorphisms in the breast cancer risk: a meta-analysis. Ther Clin Risk Manag. 2016;12:763.

39. Park HL. Epigenetic Biomarkers for Environmental Exposures and Personalized Breast Cancer Prevention. Int J Environ Res Public Health. 2020;17(4):1181.

40. Birkett N, Al-Zoughool M, Bird M, Baan RA, Zielinski J, Krewski D. Overview of biological mechanisms of human carcinogens. J Toxicol Environ Heal Part B. 2019;22(7-8):288–359.

41. Sundberg K, Dreij K, Seidel A, Jernström B. Glutathione Conjugation and DNA Adduct Formation of Dibenzo[a,l]pyrene and Benzo[a]pyrene Diol Epoxides in V79 Cells Stably Expressing Different Human Glutathione Transferases. Chem Res Toxicol. 2002;15(2):170–9.

42. Sundberg K. Differences in the catalytic efficiencies of allelic variants of glutathione transferase P1-1 towards carcinogenic diol epoxides of polycyclic aromatic hydrocarbons. Carcinogenesis. 1998;19(3):433–6.

43. Fields WR, Morrow CS, Doss AJ, Sundberg K, Jernström B, Townsend AJ. Overexpression of Stably Transfected Human Glutathione S -Transferase P1–1 Protects against DNA Damage by Benzo[a]pyrene Diol-Epoxide in Human T47D Cells. Mol Pharmacol. 1998;54(2):298–304.

44. Endo Y, Yamashita H, Takahashi S, Sato S, Yoshimoto N, Asano T, et al. Immunohistochemical determination of the miR-1290 target arylamine N-acetyltransferase 1 (NAT1) as a prognostic biomarker in breast cancer. BMC Cancer. 2014;14(1):990.

45. Li P, Butcher NJ, Minchin RF. Effect arylamine N-acetyltransferase 1 on morphology, adhesion, migration, and invasion of MDA-MB-231 cells: role of matrix metalloproteinases and integrin αV. Cell Adh Migr. 2020;14(1):1–11.

46. Carlisle SM, Trainor PJ, Doll MA, Stepp MW, Klinge CM, Hein DW. Knockout of human arylamine N -acetyltransferase 1 (NAT1) in MDA-MB-231 breast cancer cells leads to increased reserve capacity, maximum mitochondrial capacity, and glycolytic reserve capacity. Mol Carcinog. 2018;57(11):1458–66.

47. Vineis P, Bartsch H, Caporaso N, Harrington AM, Kadlubar FF, Landi MT, et al. Genetically based N-acetyltransferase metabolic polymorphism and low-level environmental exposure to carcinogens. Nature. 1994;369(6476):154–6.

48. Hein DW. Molecular genetics and function of NAT1 and NAT2: role in aromatic amine metabolism and carcinogenesis. Mutat Res Mol Mech Mutagen. 2002;506–507:65–77.

49. Wang T, Marei HE. Landscape of NAT2 polymorphisms among breast cancer. Biomed Pharmacother. 2016;77:191–6.

50. Carlisle S, Hein D. Retrospective analysis of estrogen receptor 1 and N-acetyltransferase gene expression in normal breast tissue, primary breast tumors, and established breast cancer cell lines. Int J Oncol. 2018;53(2):694–702.

51. Jernström B, Funk M, Steinbrecher T, Seidel A. Glutathione Transferase Catalyzed Conjugation of Diol Epoxides Derived from Polycyclic Aromatic Hydrocarbons with Glutathione. Polycycl Aromat Compd. 1993;3(4):213–9.

52. Dreij K, Sundberg K, Johansson A-S, Nordling E, Seidel A, Persson B, et al. Catalytic Activities of Human Alpha Class Glutathione Transferases toward Carcinogenic Dibenzo[a,l]pyrene Diol Epoxides. Chem Res Toxicol. 2002;15(6):825–31.

53. McCarty KM, Santella RM, Steck SE, Cleveland RJ, Ahn J, Ambrosone CB, et al. PAH–DNA Adducts, Cigarette Smoking, GST Polymorphisms, and Breast Cancer Risk. Environ Health Perspect. 2009;117(4):552–8.

54. Khan MKA, Akhtar S, Al-Khodairy F. Molecular docking approach to elucidate metabolic detoxification pathway of polycyclic aromatic hydrocarbons. NeuroPharmac J. 2021; 6(1): 150-161.

55. Hargis JC, Schaefer HF, Houk KN, Wheeler SE. Noncovalent interactions of a benzo[a]pyrene diol epoxide with DNA base pairs: insight into the formation of adducts of (+)-BaP DE-2 with DNA. J Phys Chem A. 2010;114(4):2038–44.

56. Ewa B, Danuta M-Š. Polycyclic aromatic hydrocarbons and PAH-related DNA adducts. J Appl Genet. 2017;58(3):321–30.

57. Genies C, Jullien A, Lefebvre E, Revol M, Maitre A, Douki T. Inhibition of the formation of benzo[a]pyrene adducts to DNA in A549 lung cells exposed to mixtures of polycyclic aromatic hydrocarbons. Toxicol Vitr. 2016;35:1–10.

58. Motwani H V., Westberg E, Törnqvist M. Interaction of benzo[a]pyrene diol epoxide isomers with human serum albumin: Site specific characterization of adducts and associated kinetics. Sci Rep. 2016;6(1):36243.

59. Cai Y, Ding S, Geacintov NE, Broyde S. Intercalative Conformations of the 14 R (+)- and 14 S (−)- trans-anti-DB[a,l]P-N 6-dA Adducts: Molecular Modeling and MD Simulations. Chem Res Toxicol. 2011;24(4):522–31.

60. Shiizaki K, Kawanishi M, Yagi T. Modulation of benzo[a]pyrene–DNA adduct formation by CYP1 inducer and inhibitor. Genes Environ. 2017;39(1):14.

61. Lukashevich O V., Baskunov VB, Darii M V., Kolbanovskiy A, Baykov AA, Gromova ES. Dnmt3a-CD Is Less Susceptible to Bulky Benzo[a]pyrene Diol Epoxide-Derived DNA Lesions Than Prokaryotic DNA Methyltransferases. Biochemistry. 2011;50(5):875–81.

62. Dipple A, Pigott MA, Agarwal SK, Yagi H, Sayer JM, Jerina DM. Optically active benzo[c]phenanthrene diol epoxides bind extensively to adenine in DNA. Nature. 1987;327(6122):535–6.

63. Arif JM, Smith WA, Gupta RC. Tissue distribution of DNA adducts in rats treated by intramammillary injection with dibenzo[a,l]pyrene, 7,12-dimethylbenz[a]anthracene and benzo[a]pyrene. Mutat Res Mol Mech Mutagen. 1997;378(1–2):31–9.

64. Khan MKA, Akhtar S, Arif JM. Development of In Silico Protocols to Predict Structural Insights into the Metabolic Activation Pathways of Xenobiotics. Interdiscip Sci Comput Life Sci. 2018;10(2):329–45.

65. Ahmad KMK, Salman A, Al-Khodairy Salman F, Al-Marshad Feras M, Alshahrani Abdulrahman M, Arif Jamal M. Computational Exploration of Dibenzo[a,l]Pyrene Interaction to DNA and its Bases: Possible Implications to Human Health. Biointerface Res Appl Chem. 2020;11(4):11272–83.

66. Dreij K, Seidel A, Jernström B. Differential Removal of DNA Adducts Derived from anti -Diol Epoxides of Dibenzo[a,l]pyrene and Benzo[a]pyrene in Human Cells. Chem Res Toxicol. 2005;18(4):655–64.

67. Ruan Q, Kolbanovskiy A, Zhuang P, Chen J, Krzeminski J, Amin S, et al. Synthesis and Characterization of Site-Specific and Stereoisomeric Fjord Dibenzo[a,l]pyrene Diol Epoxide-N 6-Adenine Adducts: Unusual Thermal Stabilization of Modified DNA Duplexes. Chem Res Toxicol. 2002;15(2):249–61.

68. Zhong Q, Amin S, Lazarus P, Spratt TE. Differential repair of polycyclic aromatic hydrocarbon DNA adducts from an actively transcribed gene. DNA Repair (Amst). 2010;9(9):1011–6.

69. Shafirovich V, Kolbanovskiy M, Kropachev K, Liu Z, Cai Y, Terzidis MA, et al. Nucleotide Excision Repair and Impact of Site-Specific 5',8-Cyclopurine and Bulky DNA Lesions on the Physical Properties of Nucleosomes. Biochemistry. 2019;58(6):561-74.

70. Gelhaus SL, Harvey RG, Penning TM, Blair IA. Regulation of benzo[a]pyrene-mediated DNA- and glutathione-adduct formation by 2,3,7,8-tetrachlorodibenzo-p-dioxin in human lung cells. Chem Res Toxicol. 2011;24(1):89–98.

71. Cai Y, Geacintov NE, Broyde S. Nucleotide Excision Repair Efficiencies of Bulky Carcinogen–DNA Adducts Are Governed by a Balance between Stabilizing and Destabilizing Interactions. Biochemistry. 2012;51(7):1486–99.

72. Bock FJ, Tait SWG. Mitochondria as multifaceted regulators of cell death. Nat Rev Mol Cell Biol. 2020;21(2):85–100.

73. Bock FJ, Tait SWG. Mitochondria as multifaceted regulators of cell death. Nat Rev Mol Cell Biol. 2020;21(2):85–100.

74. Kale J, Osterlund EJ, Andrews DW. BCL-2 family proteins: changing partners in the dance towards death. Cell Death Differ. 2018;25(1):65–80.

75. Czabotar PE, Lessene G, Strasser A, Adams JM. Control of apoptosis by the BCL-2 protein family: implications for physiology and therapy. Nat Rev Mol Cell Biol. 2014;15(1):49–63.

76. Warren CFA, Wong-Brown MW, Bowden NA. BCL-2 family isoforms in apoptosis and cancer. Cell Death Dis. 2019;10(3):177.

77. Bogner C, Kale J, Pogmore J, Chi X, Shamas-Din A, Fradin C, et al. Allosteric Regulation of BH3 Proteins in Bcl-xL Complexes Enables Switch-like Activation of Bax. Mol Cell. 2020;77(4):901-912.

78. Ouyang L, Shi Z, Zhao S, Wang F-T, Zhou T-T, Liu B, et al. Programmed cell death pathways in cancer: a review of apoptosis, autophagy and programmed necrosis. Cell Prolif. 2012;45(6):487–98.

79. Jan R, Chaudhry G-S. Understanding Apoptosis and Apoptotic Pathways Targeted Cancer Therapeutics. Adv Pharm Bull. 2019;9(2):205–18.

80. Guo Z, Song T, Wang Z, Lin D, Cao K, Liu P, et al. The chaperone Hsp70 is a BH3 receptor activated by the pro-apoptotic Bim to stabilize anti-apoptotic clients. J Biol Chem. 2020;295(37):12900–9.

81. Huang K, O'Neill KL, Li J, Zhou W, Han N, Pang X, et al. BH3-only proteins target BCL-xL/MCL-1, not BAX/BAK, to initiate apoptosis. Cell Res. 2019;29(11):942–52.

82. Yin C, Knudson CM, Korsmeyer SJ, Dyke T Van. Bax suppresses tumorigenesis and stimulates apoptosis in vivo. Nature. 1997;385(6617):637–40.

83. Oda E. Noxa, a BH3-Only Member of the Bcl-2 Family and Candidate Mediator of p53-Induced Apoptosis. Science. 2000;288(5468):1053–8.

84. Oda K, Arakawa H, Tanaka T, Matsuda K, Tanikawa C, Mori T, et al. p53AIP1, a Potential Mediator of p53-Dependent Apoptosis, and Its Regulation by Ser-46-Phosphorylated p53. Cell. 2000;102(6):849–62.

85. Kracikova M, Akiri G, George A, Sachidanandam R, Aaronson SA. A threshold mechanism mediates p53 cell fate decision between growth arrest and apoptosis. Cell Death Differ. 2013;20(4):576–88.

86. Hegeman SA, Ghannouma H, Zhou L. Role of p53-Mediated Apoptosis in Limiting Metastasis. UF J Undergrad Res. 2020;21(2).

87. Soengas MS. Apaf-1 and Caspase-9 in p53-Dependent Apoptosis and Tumor Inhibition. Science. 1999;284(5411):156–9.

88. Soengas MS. Apaf-1 and Caspase-9 in p53-Dependent Apoptosis and Tumor Inhibition. Science. 1999;284(5411):156–9.

89. Duffy MJ, Synnott NC, Crown J. Mutant p53 in breast cancer: potential as a therapeutic target and biomarker. Breast Cancer Res Treat. 2018;170(2):213–9.

90. Irwin M, Marin MC, Phillips AC, Seelan RS, Smith DI, Liu W, et al. Role for the p53 homologue p73 in E2F-1-induced apoptosis. Nature. 2000;407(6804):645–8.

91. Helin K, Harlow E, Fattaey A. Inhibition of E2F-1 transactivation by direct binding of the retinoblastoma protein. Mol Cell Biol. 1993;13(10):6501–8.

92. Christensen J. Characterization of E2F8, a novel E2F-like cell-cycle regulated repressor of E2F-activated transcription. Nucleic Acids Res. 2005;33(17):5458–70.

93. Nahle Z, Polakoff J, Davuluri R V., McCurrach ME, Jacobson MD, Narita M, et al. Direct coupling of the cell cycle and cell death machinery by E2F. Nat Cell Biol. 2002;4(11):859–64.

94. Akl H, Vervloessem T, Kiviluoto S, Bittremieux M, Parys JB, De Smedt H, et al. A dual role for the anti-apoptotic Bcl-2 protein in cancer: Mitochondria versus endoplasmic reticulum. Biochim Biophys Acta - Mol Cell Res. 2014;1843(10):2240–52.

95. Khan MKA, Akhtar S, Arif JM. Structural Insight into the Mechanism of Dibenzo[a,l]pyrene and Benzo[a]pyrene-Mediated Cell Proliferation Using Molecular Docking Simulations. Interdiscip Sci Comput Life Sci. 2018;10(4):653–73.

96. Anifowose AJ, Ogundola AO, Babalola BM, Awojide SH. Measurement, Source-Profiling and Potential Toxicity of Polycyclic Aromatic Hydrocarbons in an Agrarian Soil. Environ Process. 2020;7(3):827–44.

97. Jeffery J, Carradus M, Songin K, Pettit M, Pettit K, Wright C. Optimized method for determination of 16 FDA polycyclic aromatic hydrocarbons (PAHs) in mainstream cigarette smoke by gas chromatography–mass spectrometry. Chem Cent J. 2018;12(1):27.

98. Mescher M, Haarmann-Stemmann T. Modulation of CYP1A1 metabolism: From adverse health effects to chemoprevention and therapeutic options. Pharmacol Ther. 2018;187:71–87.

99. Beck TC, Beck KR, Morningstar J, Benjamin MM, Norris RA. Descriptors of Cytochrome Inhibitors and Useful Machine Learning Based Methods for the Design of Safer Drugs. Pharmaceuticals. 2021;14(5):472.

100. Luch A, Schober W, Soballa VJ, Raab G, Greim H, Jacob J, et al. Metabolic Activation of Dibenzo[a,l]pyrene by Human Cytochrome P450 1A1 and P450 1B1 Expressed in V79 Chinese Hamster Cells. Chem Res Toxicol. 1999;12(4):353–64.

101. Smith JN, Mehinagic D, Nag S, Crowell SR, Corley RA. In vitro metabolism of benzo[a]pyrene-7,8-dihydrodiol and dibenzo[def,p]chrysene-11,12 diol in rodent and human hepatic microsomes. Toxicol Lett. 2017;269:23–32.

102. Shimada T. Inhibition of Carcinogen-Activating Cytochrome P450 Enzymes by Xenobiotic Chemicals in Relation to Antimutagenicity and Anticarcinogenicity. Toxicol Res. 2017;33(2):79–96.

103. Siddens LK, Larkin A, Krueger SK, Bradfield CA, Waters KM, Tilton SC, et al. Polycyclic aromatic hydrocarbons as skin carcinogens: Comparison of

benzo[a]pyrene, dibenzo[def,p]chrysene and three environmental mixtures in the FVB/N mouse. Toxicol Appl Pharmacol. 2012;264(3):377–86.

104. Manikandan P, Nagini S. Cytochrome P450 Structure, Function and Clinical Significance: A Review. Curr Drug Targets. 2018;19(1):38–54.

105. Munro AW, McLean KJ, Grant JL, Makris TM. Structure and function of the cytochrome P450 peroxygenase enzymes. Biochem Soc Trans. 2018;46(1):183–96.

106. Barnaba C, Gentry K, Sumangala N, Ramamoorthy A. The catalytic function of cytochrome P450 is entwined with its membrane-bound nature. F1000Research. 2017;6:662.

107. Rendic SP, Guengerich FP. Human Family 1–4 cytochrome P450 enzymes involved in the metabolic activation of xenobiotic and physiological chemicals: an update. Arch Toxicol. 2021;95(2):395–472.

108. Nakano N, Sakata N, Katsu Y, Nochise D, Sato E, Takahashi Y, et al. Dissociation of the AhR/ARNT complex by TGF-β/Smad signaling represses CYP1A1 gene expression and inhibits benze[a]pyrene-mediated cytotoxicity. J Biol Chem. 2020;295(27):9033–51.

109. Androutsopoulos VP, Tsatsakis AM, Spandidos DA. Cytochrome P450 CYP1A1: wider roles in cancer progression and prevention. BMC Cancer [Internet]. 2009 Dec 16;9(1):187.

110. Lemkul JA. Pairwise-additive and polarizable atomistic force fields for molecular dynamics simulations of proteins. In: Progress in Molecular Biology and Translational Science. 2020. p. 1–71.

111. Kim S, Lee J, Jo S, Brooks CL, Lee HS, Im W. CHARMM-GUI ligand reader and modeler for CHARMM force field generation of small molecules. J Comput Chem. 2017 ;38(21):1879–86.

112. Van Den Driessche G, Fourches D. Adverse drug reactions triggered by the common HLA-B*57:01 variant: virtual screening of DrugBank using 3D molecular docking. J Cheminfor. 2018;10(1):3.

113. Zoete V, Daina A, Bovigny C, Michielin O. SwissSimilarity: A Web Tool for Low to Ultra High Throughput Ligand-Based Virtual Screening. J Chem Inf Model. 2016 56(8):1399–404.

114. Lipinski CA. Lead- and drug-like compounds: the rule-of-five revolution. Drug Discov Today Technol. 2004;1(4):337–41.

115. Tan H-Y, Trier S, Rahbek UL, Dufva M, Kutter JP, Andresen TL. A multi-chamber microfluidic intestinal barrier model using Caco-2 cells for drug transport studies. Deli MA, editor. PLoS One. 2018;13(5):e0197101.

116. Zhu J, Yi X, Zhang J, Chen S, Wu Y. Rapid screening of brain-penetrable antioxidants from natural products by blood-brain barrier specific permeability assay combined with DPPH recognition. J Pharm Biomed Anal. 2018;151:42–8.

117. Liu W, Jiang X, Zu Y, Yang Y, Liu Y, Sun X, et al. A comprehensive description of GluN2B-selective N-methyl-D-aspartate (NMDA) receptor antagonists. Eur J Med Chem. 2020;200:112447.

118. Morris GM, Goodsell DS, Halliday RS, Huey R, Hart WE, Belew RK, et al. Automated docking using a Lamarckian genetic algorithm and an empirical binding free energy function. J Comput Chem. 1998;19(14):1639–62.

119. Morris GM, Goodsell DS, Huey R, Olson AJ. Distributed automated docking of flexible ligands to proteins: Parallel applications of AutoDock 2.4. J Comput Aided Mol Des. 1996;10(4):293–304.

120. Khan FI, Lai D, Anwer R, Azim I, Khan MKA. Identifying novel sphingosine kinase 1 inhibitors as therapeutics against breast cancer. J Enzyme Inhib Med Chem. 2020;35(1):172–86.

121. Khan S, Khan FI, Mohammad T, Khan P, Hasan GM, Lobb KA, et al. Exploring molecular insights into the interaction mechanism of cholesterol derivatives with the Mce4A: A combined spectroscopic and molecular dynamic simulation studies. Int J Biol Macromol. 2018;111:548–60.

122. Gunasekaran D, Sridhar J, Suryanarayanan V, Manimaran NC, Singh SK. Molecular modeling and structural analysis of nAChR variants uncovers the mechanism of resistance to snake toxins. J Biomol Struct Dyn. 2017;35(8):1654–71.

123. Naz F, Khan FI, Mohammad T, Khan P, Manzoor S, Hasan GM, et al. Investigation of molecular mechanism of recognition between citral and MARK4: A newer therapeutic approach to attenuate cancer cell progression. Int J Biol Macromol. 2018;107(Pt B):2580–9.

124. Mosmann T. Rapid colorimetric assay for cellular growth and survival: Application to proliferation and cytotoxicity assays. J Immunol Methods. 1983;65(1–2):55–63.

125. Alreshidi FS, Ginawi IA, Hussain MA, Arif JM. Piperaquine- and Aspirin- Mediated Protective Role of HSP70 and HSP90 as Modes to Strengthen the Natural

Immunity against Potent SARS-CoV-2. Biointerface Res Appl Chem. 2021;11(4):12364–79.

126. Laskowski RA, Swindells MB. LigPlot+: Multiple Ligand–Protein Interaction Diagrams for Drug Discovery. J Chem Inf Model. 2011;51(10):2778–86.

127. Baildya N, Khan AA, Ghosh NN, Dutta T, Chattopadhyay AP. Screening of potential drug from Azadirachta Indica (Neem) extracts for SARS-CoV-2: An insight from molecular docking and MD-simulation studies. J Mol Struct. 2021;1227:129390.

128. Naz S, Farooq U, Khan S, Sarwar R, Mabkhot YN, Saeed M, et al. Pharmacophore model-based virtual screening, docking, biological evaluation and molecular dynamics simulations for inhibitors discovery against α -tryptophan synthase from Mycobacterium tuberculosis. J Biomol Struct Dyn. 2021;39(2):610–20.

129. Hargis JC, III HFS, Houk KN, Wheeler SE. Noncovalent Interactions of a Benzo[a]pyrene Diol Epoxide with DNA Base Pairs: Insight into the Formation of Adducts of (+)-BaPDE-2 with DNA. J Phys Chem A. 2010;114(4):2038–44.

130. Ewa B, Danuta M-Š. Polycyclic aromatic hydrocarbons and PAH-related DNA adducts. J Appl Genet. 2017;58(3):321–30.

131. Genies C, Jullien A, Lefebvre E, Revol M, Maitre A, Douki T. Inhibition of the formation of benzo[a]pyrene adducts to DNA in A549 lung cells exposed to mixtures of polycyclic aromatic hydrocarbons. Toxicol Vitr. 2016;35:1–10.

132. Motwani H V., Westberg E, Törnqvist M. Interaction of benzo[a]pyrene diol epoxide isomers with human serum albumin: Site specific characterisation of adducts and associated kinetics. Sci Rep. 2016;6(1):36243.

133. Cai Y, Ding S, Geacintov NE, Broyde S. Intercalative Conformations of the 14 R (+)- and 14 S (−)- trans-anti-DB[a,l]P-N 6-dA Adducts: Molecular Modeling and MD Simulations. Chem Res Toxicol. 2011;24(4):522–31.

134. Shiizaki K, Kawanishi M, Yagi T. Modulation of benzo[a]pyrene–DNA adduct formation by CYP1 inducer and inhibitor. Genes Environ. 2017;39(1):14.

135. Lukashevich O V., Baskunov VB, Darii M V., Kolbanovskiy A, Baykov AA, Gromova ES. Dnmt3a-CD Is Less Susceptible to Bulky Benzo[a]pyrene Diol Epoxide-Derived DNA Lesions Than Prokaryotic DNA Methyltransferases. Biochemistry. 2011;50(5):875–81.

136. Dipple A, Pigott MA, Agarwal SK, Yagi H, Sayer JM, Jerina DM. Optically active benzo[c]phenanthrene diol epoxides bind extensively to adenine in DNA. Nature. 1987;327(6122):535–6.

137. Ralston SL, Seidel A, Luch A, Platt KL, Baird WM. Stereoselective activation of dibenzo[a,l]pyrene to (—)- anti (11 R,12 S,13S,14 R)- and (+)- syn (11S, 12R, 13S,14R)- 11,12-diol-13,14-epoxides which bind extensively to deoxyadenosine residues of DNA in the human mammary carcinoma. Carcinogenesis. 1995;16(12):2899–907.

138. Rodríguez FA, Liu Z, Lin CH, Ding S, Cai Y, Kolbanovskiy A, et al. Nuclear Magnetic Resonance Studies of an N2-Guanine Adduct Derived from the Tumorigen Dibenzo[a,l]pyrene in DNA: Impact of Adduct Stereochemistry, Size, and Local DNA Sequence on Solution Conformations. Biochemistry. 2014;53(11):1827–41.

139. Kropachev K, Kolbanovskiy M, Liu Z, Cai Y, Zhang L, Schwaid AG, et al. Adenine–DNA Adducts Derived from the Highly Tumorigenic Dibenzo[a,l]pyrene Are Resistant to Nucleotide Excision Repair while Guanine Adducts Are Not. Chem Res Toxicol. 2013;26(5):783–93.

140. Spivak G. Nucleotide excision repair in humans. DNA Repair (Amst). 2015;36:13–8.

141. Kropachev K, Kolbanovskiy M, Liu Z, Cai Y, Zhang L, Schwaid AG, et al. Adenine–DNA Adducts Derived from the Highly Tumorigenic Dibenzo[a,l]pyrene Are Resistant to Nucleotide Excision Repair while Guanine Adducts Are Not. Chem Res Toxicol. 2013;26(5):783–93.

142. Cortez D. Preventing replication fork collapse to maintain genome integrity. DNA Repair (Amst). 2015;32:149–57.

143. Sugasawa K. Molecular mechanisms of DNA damage recognition for mammalian nucleotide excision repair. DNA Repair (Amst). 2016;44:110–7.

144. 1Stingele J, Bellelli R, Boulton SJ. Mechanisms of DNA–protein crosslink repair. Nat Rev Mol Cell Biol. 2017;18(9):563–73.

145. Marteijn JA, Lans H, Vermeulen W, Hoeijmakers JHJ. Understanding nucleotide excision repair and its roles in cancer and ageing. Nat Rev Mol Cell Biol. 2014;15(7):465–81.

146. Zha J, Harada H, Osipov K, Jockel J, Waksman G, Korsmeyer SJ. BH3 Domain of BAD Is Required for Heterodimerization with BCL-XL and Pro-apoptotic Activity. J Biol Chem. 1997;272(39):24101–4.

147. Korsmeyer SJ, Yin X-M, Yang E, Zha J, Sedlak T, Oltvai Z. BCL-2 gene family and the regulation of programmed cell death. Cancer Genet Cytogenet. 1995;84(2):138.

148. Tilokani L, Nagashima S, Paupe V, Prudent J. Mitochondrial dynamics: overview of molecular mechanisms. Garone C, Minczuk M, editors. Essays Biochem. 2018;62(3):341–60.

149. Tanaka T. Role of Apoptosis in the Chemoprevention of Cancer. J Exp Clin Med. 2013;5(3):89–91.

150. Widden H, Kaczmarczyk A, Subedi A, Whitaker RH, Placzek WJ. MCL1 binds and negatively regulates the transcriptional function of tumor suppressor p73. Cell Death Dis. 2020;11(11):946.

151. Smith VM, Dietz A, Henz K, Bruecher D, Jackson R, Kowald L, et al. Specific interactions of BCL-2 family proteins mediate sensitivity to BH3-mimetics in diffuse large B-cell lymphoma. Haematologica. 2020;105(8):2150–63.

152. Stefanski CD, Keffler K, McClintock S, Milac L, Prosperi JR. APC loss affects DNA damage repair causing doxorubicin resistance in breast cancer cells. Neoplasia. 2019;21(12):1143–50.

153. Allende-Vega N, Krzywinska E, Orecchioni S, Lopez-Royuela N, Reggiani F, Talarico G, et al. The presence of wild type p53 in hematological cancers improves the efficacy of combinational therapy targeting metabolism. Oncotarget. 2015;6(22):19228–45.

154. Ajijur R, Salman A, Ahmad KMK. Combinatorial Design to Decipher Novel Lead Molecule against Mycobacterium tuberculosis. Biointerface Res Appl Chem. 2021;11(5):12993–3004.

155. Cavalieri EL, Devanesan P, Bosland MC, Badawi AF, Rogan EG. Catechol estrogen metabolites and conjugates in different regions of the prostate of Noble rats treated with 4-hydroxyestradiol: implications for estrogen-induced initiation of prostate cancer. Carcinogenesis. 2002;23(2):329–33.

156. Takemura H, Uchiyama H, Ohura T, Sakakibara H, Kuruto R, Amagai T, et al. A methoxyflavonoid, chrysoeriol, selectively inhibits the formation of a carcinogenic estrogen metabolite in MCF-7 breast cancer cells. J Steroid Biochem Mol Biol. 2010;118(1–2):70–6.

157. Iwata H, Yamaguchi K, Takeshita Y, Kubota A, Hirakawa S, Isobe T, et al. Enzymatic characterization of in vitro -expressed Baikal seal cytochrome P450 (CYP) 1A1, 1A2, and 1B1: Implication of low metabolic potential of CYP1A2 uniquely evolved in aquatic mammals. Aquat Toxicol. 2015;162:138–51.

158. Dong J, Huang G, Zhang Q, Wang Z, Cui J, Wu Y, et al. Development of benzochalcone derivatives as selective CYP1B1 inhibitors and anticancer agents. Medchemcomm. 2019;10(9):1606–14.

159. Dutkiewicz Z, Mikstacka R. Structure-Based Drug Design for Cytochrome P450 Family 1 Inhibitors. Bioinorg Chem Appl. 2018;2018:1–21.

160. Dong J, Huang G, Cui Q, Meng Q, Li S, Cui J. Discovery of heterocycle-containing α-naphthoflavone derivatives as water-soluble, highly potent and selective CYP1B1 inhibitors. Eur J Med Chem. 2021;209:112895.

161. Datta A, Bhasin N, Kim H, Ranjan M, Rider B, Abd Elmageed ZY, et al. Selective targeting of FAK–Pyk2 axis by alpha-naphthoflavone abrogates doxorubicin resistance in breast cancer cells. Cancer Lett. 2015;362(1):25–35.

162. Osmaniye D, Korkut Çelikateş B, Sağlık BN, Levent S, Acar Çevik U, Kaya Çavuşoğlu B, et al. Synthesis of some new benzoxazole derivatives and investigation of their anticancer activities. Eur J Med Chem. 2021;210:112979.

163. Surichan S, Arroo RR, Tsatsakis AM, Androutsopoulos VP. Tangeretin inhibits the proliferation of human breast cancer cells via CYP1A1/CYP1B1 enzyme induction and CYP1A1/CYP1B1–mediated metabolism to the product 4′ hydroxy tangeretin. Toxicol Vitr. 2018;50:274–84.

164. Wójcikowski J, Danek PJ, Basińska-Ziobroń A, Pukło R, Daniel WA. In vitro inhibition of human cytochrome P450 enzymes by the novel atypical antipsychotic drug asenapine: a prediction of possible drug–drug interactions. Pharmacol Reports. 2020;72(3):612–21.

165. Shimada T, Guengerich FP. Inhibition of Human Cytochrome P450 1A1-, 1A2-, and 1B1-Mediated Activation of Procarcinogens to Genotoxic Metabolites by Polycyclic Aromatic Hydrocarbons. Chem Res Toxicol. 2006;19(2):288–94.

166. Juvonen RO, Jokinen EM, Javaid A, Lehtonen M, Raunio H, Pentikäinen OT. Inhibition of human CYP1 enzymes by a classical inhibitor α-naphthoflavone and a novel inhibitor N-(3, 5-dichlorophenyl) cyclopropane carboxamide: An in vitro and in silico study. Chem Biol Drug Des. 2020;95(5):520–33.